AG-336

4. BOUNDARY MEASUREMENTS METHODS

Authors : P.Ashill (Chapter 4.1, 4.2)
J.E. Hackett (Chapter 4.2)
M. Mokry (Chapter 4.3)
F. Steinle (Chapter 4.3

PAGE

4. BOUNDARY MEASUREMENTS METHODS

The importance of measuring flow conditions at outer boundaries has been known for some time, particularly for solid-wall wind tunnels. However, it has only been in recent years that sufficient computing power has become available to make use of this information. Thus it is no coincidence that the increase in interest in boundary-measurement methods has occurred during the last decade or so when the rate of development in computing technology has been so rapid. This Chapter begins with a review of fundamental theories of boundary-measurement methods (Chapter 4.1) and then describes the application of the methods to closed-wall tunnels in Chapter 4.2 and to ventilated test sections in Chapter 4.3.

4.1 FUNDAMENTAL THEORIES

After basic issues are considered, the various classes of methods are reviewed, and the relative advantages and disadvantages of the methods are discussed.

LIST OF SYMBOLS for chapter 4.1

B	breadth of working section of equivalent wind tunnel of rectangular section
C_p	static-pressure coefficient
G, G_D, G_F	Green's functions
G_N, G_{DN}	
H	height of working section of equivalent wind tunnel of rectangular section
M	Mach number
n	normal inward towards working section in transformed (Prandtl-Glauert) space
P	point within region bounded by S
R	fictitious region outside the region bounded by S
S	measurement surface in transformed space
T	wall shape factor for doublet
u	streamwise velocity perturbation
U	stream speed
V	model volume
x,y,z	cartesian co-ordinate system (Fig 4.1)
X,Y,Z	transformed co-ordinates, = (x, βy, βz)
α	angle of incidence
β	Prandtl-Glauert factor, = $\sqrt{(1 - M_F^2)}$
δ_0, δ_1	lift interference parameters
Δ	increment due to wall effect
∇^2	Laplace operator
Φ	velocity potential
φ	perturbation velocity potential

SUFFIXES

F	equivalent free-air flow
I	wall-induced flow
i,j	differentiation with respect to either x,y or z in either case
R	fictitious region outside region contained within S
S	measurement surface
T	adjacent to wind-tunnel walls
U, D	upstream and downstream faces
V_0	volume integration in the fictitious region R
∞	conditions far upstream

4.1.1 BASIC CONSIDERATIONS

Consider the flow about a model of an aircraft in a wind tunnel (Figure 4.1) with sub-sonic conditions far upstream. Suppose, initially, that the flow everywhere in the working section is irrotational, implying that any shock waves are weak and that the turbulent shear layers are thin. The flow may therefore be defined uniquely by the velocity potential Φ or the perturbation velocity potential $\varphi = \Phi - U_\infty x$, where U_∞ is the speed

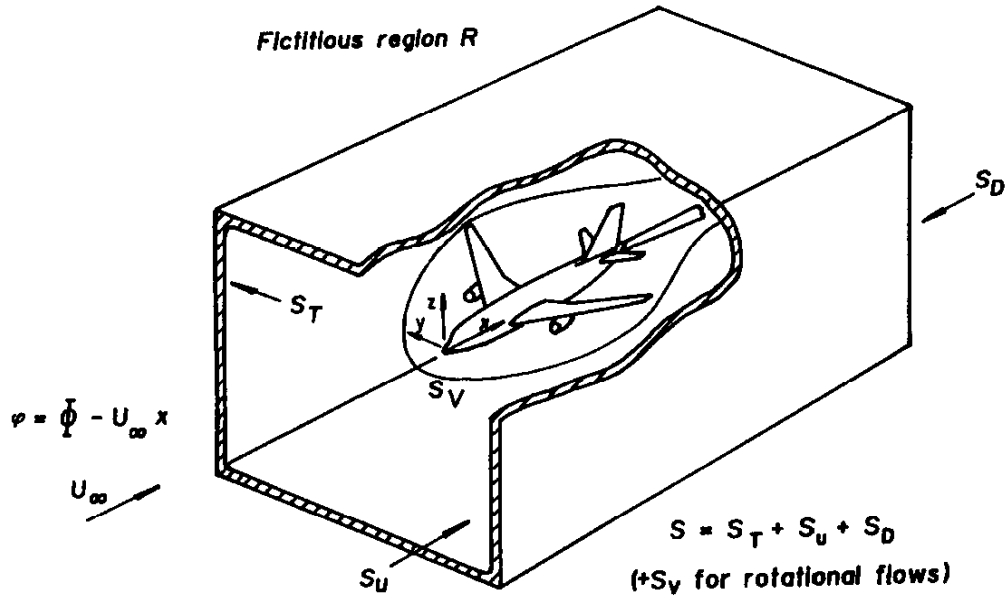

Figure 4.1 : Wind Tunnel Test Section with Model

of the notional flow far upstream, usually determined by calibration of the empty test section. This flow satisfies the exact potential equation (Küchemann, [27]), which may be written in the form :

$$\beta^2 \varphi_{xx} + \varphi_{yy} + \varphi_{zz} = f(\Phi_i, \Phi_{ij}, U_F; M_F), \qquad (4.1)$$

where $\beta^2 = 1 - M_F^2$ and M_F is the Mach number corrected for blockage, i.e. the free-stream Mach number of an equivalent 'free-air' flow. The corrected Mach number and the corresponding corrected free-stream speed, U_F, are preferred in Equation (4.1) to the corresponding conditions far upstream because the former quantities

determine the character of the flow in the near field of the model. Suffixes i and j, respectively, refer to differentiation with respect to either x, y or z. The function f is a term that is non-linear in the derivatives of F and which becomes significant in transonic-flow regions near the model.

The Prandtl-Glauert transformation may be used to replace Equation (4.1) by

$$\nabla^2 \varphi = f\left(\Phi_i , \Phi_{ij} , U_F , M_F \right) / \beta^2 \qquad (4.2)$$

where

$$\nabla^2 \varphi = \varphi_{xx} + \varphi_{yy} + \varphi_{zz}$$

and

$$(X,\ Y,\ Z) = (x,\ \beta y,\ \beta z).$$

Consider now the 'free-air' flow about the same model at the free-stream speed U_F and at an angle of attack differing from the geometric angle of attack of the model in the tunnel by $\Delta\alpha$ (Figure 4.2). For flows and models with a vertical plane of symmetry this flow is characterised by the perturbation potential

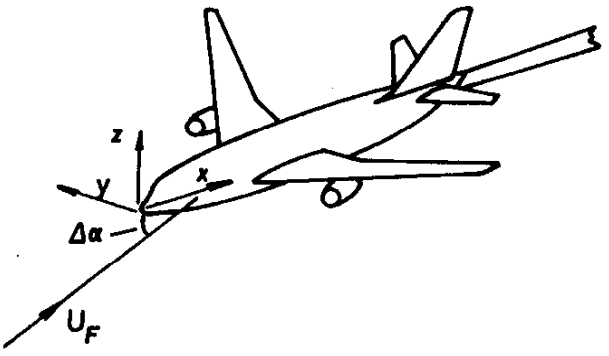

Fig 4.2 Free-air flow about same model

$$\varphi_F = \Phi_F - U_F x - U_F \Delta\alpha z$$

and satisfies the equation

$$\Delta^2 \varphi_F = f\left[(\Phi_F)_i , (\Phi_F)_{ij} , U_F ; M_F\right] / \beta^2 \qquad (4.3)$$

If either

a) the two flows are identical ($\Phi = \Phi_F$) in the region near the model, so that the tunnel flow may be corrected to an equivalent 'free-air' flow,

or **b)** the perturbations in the flow induced by the model are 'small' everywhere,

or **c)** the Mach number of the flow is everywhere close to zero, i.e. the two flows are essentially incompressible, then the right-hand sides of Equations (4.2) and (4.3) are either identical but non-zero, or negligible. This being the case, subtraction of Equation (4.3) from Equation (4.2) leads to the expression

$$\nabla^2 \varphi = 0 \qquad (4.4)$$

where $\varphi_I = \varphi - \varphi_F$

is the wall-interference potential. Since, by Equation (4.4), this potential is harmonic within the working section, it is possible to use Green's formula (Weatherburn, [51]) to write for the point P in the (transformed) working section

$$4\pi \varphi_I (P) = -\int_S \left[\frac{\partial \varphi_I}{\partial n} G - \varphi_I \frac{\partial G}{\partial n}\right] dS, = -\int_S \left(\left[\frac{\partial \varphi}{\partial n} - \frac{\partial \varphi_F}{\partial n}\right] G - (\varphi - \varphi_F)\frac{\partial G}{\partial n}\right) dS. \qquad (4.5)$$

Here n is the normal inward towards the working section and the integration is performed over the measurement or boundary surface S, comprising a surface at or close to the walls, S_T, with faces at the upstream and downstream extremities of the working section, S_U and S_D, (Figure 4.1). G is a Green's function that is harmonic everywhere within the measurement region except at the point P. Near this point G behaves like 1/r, where r is the distance between the point P and a variable point in the region.

For the wall interference potential to be harmonic everywhere within the volume bounded by S the quantity (φ - φ_F) must be single-valued there. This means that the difference in circulation between the two flows around any circuit within the working section must be zero and, also,

$$\int_S \left(\frac{\partial \varphi}{\partial n} - \frac{\partial \varphi_F}{\partial n} \right) dS = 0,$$

i.e., to the accuracy of linear theory, the net flux of the wall-induced flow across S must be zero. These conditions need to be borne in mind in any numerical method for determining wall interference based on Equation (4.5).

The analysis above may, with certain restrictions, be extended to rotational flows. The first restriction is that the vorticity is confined to a region surrounding the model, as illustrated in Figure 4.1, where it is shown to be bounded by the surface S_V. The surface S in Equation (4.5) then has to include the surface S_V. However, if it is possible to correct the wind tunnel flow to an equivalent free-air flow, the analytical continuation of the wall-interference potential is harmonic within the rotational-flow region. Hence, by Green's theorem (Weatherburn, [51]), the contribution of the extra term vanishes. Thus, in this circumstance, Equation (4.5) applies to rotational flows as well.

To determine the wall-interference potential at a point in the working section by using Equation (4.5), it is necessary to know both the wall interference potential itself and its normal gradient at the measurement surface. This, in turn, means that perturbation potential of the wind-tunnel flow and its normal gradient have to be determined at the surface; furthermore, a satisfactory representation of the free-air flow around the model has to be derived. This implies that three independent variables are required, two from flow measurements at the surface S and a third, defining the model free-air flow, by calculation. However, the number of variables needed can be reduced to two by using the freedom to choose an appropriate Green's function for the boundary-value problem. Depending on the choice of Green's function, the two variables can either comprise one defining the flow at any one part of the measurement surface and another specifying the free-air flow or two defining the conditions at the measurement surface. Kraft [25] suggested that a measure of merit of any technique is how well the two independent quantities are evaluated. Kraft proposed that the two classes of method should be, respectively, called 'one-variable' and 'two-variable' methods. As its name implies, the former class needs the measurement of only one flow variable at the measurement surface, but it does require a representation of the model free-air flow. The second class, on the other hand, requires two variables to be measured, but it does not need a simulation of the model flow. A third, hybrid class uses a) a complete knowledge of one flow variable, or an assumed relationship between the two flow variables, at the measurement surface, and b) limited measurements of a second flow variable on the same surface. In these 'wall-signature' methods, a model representation is used, and the 'signature' of the second variable is used to define either the strengths of the singularities representing the model or the values of a parameter linking the two flow variables. In the remainder of this Chapter the three types of methods are reviewed. Discussion of one-variable methods (Chapter 4.1.2) is followed by a review of 'wall-signature' methods (Chapter 4.1.3). Finally, two-variable methods are discussed in Chapter 4.1.4.

4.1.2 ONE VARIABLE METHODS

4.1.2.1 DIRICHLET PROBLEM

For the Dirichlet problem, where the interference potential is specified on S, the appropriate Green's function is one that vanishes on the measurement surface leaving

$$4\pi \varphi_I(P) = \int_S (\varphi - \varphi_F) \frac{\partial G_D}{\partial n} dS. \qquad (4.6)$$

With the appropriate Green's function, G_D, defined, the integral can, in principle, be evaluated once the perturbation potentials φ and φ_F are known on S. The perturbation potential φ can, in principle, be inferred from

i) measurements of static pressure at the outside surface S_T by appropriate integration of the linearised version of Bernoulli's equation,

$$\frac{\partial \varphi}{\partial x} = - \frac{U_\infty C_p}{2}, \qquad (4.7)$$

provided that the pressure coefficient C_p is of sufficiently small magnitude for second order terms in Bernoulli's equation to be ignored [1], and

ii) a knowledge of the way the perturbation velocity potential varies across the upstream and downstream faces S_U and S_D. If these surfaces are perpendicular to the tunnel axis this variation can be determined by measurement of the upwash component of velocity at these faces. However, for sufficiently long working sections, where the two faces are far removed from the model, this is probably unnecessary because the contributions of the integrals over these faces can reasonably be ignored.

The integration of Equation (4.7) has been avoided in existing methods of the 'Dirichlet' type, which are based on the streamwise velocity increment $u = \partial\varphi/\partial x$ instead of the perturbation velocity potential φ. However, in these methods, a further integration is needed to determine the wall-induced upwash, and the constant of integration is determined from a measurement of the upwash at the upstream measurement station. The alternative expressions have been derived for cylindrical boundary surfaces. For these types of surfaces, a comparable expression may be derived from Equation (4.6) by differentiating each side of this equation by X. Mokry and Ohman [36], in two dimensions, and Mokry [38], in three dimensions, used Fourier transform techniques, in effect, to determine the required Green's function. Later, Mokry et al [40] used a doublet-panel method, in which the doublet distribution on the measurement surface is determined satisfying the boundary condition for the wall-induced increment in streamwise velocity. In all these methods, the influence of the upstream and downstream faces can, in principle, be accommodated provided information about the variation of the streamwise increment in velocity across them is available. In an analysis of the two-dimensional problem in a working section of infinite length, Capelier et al [7] used complex-variable theory to solve the equivalent Schwarz problem (Mokry et al [39]). An extension of this method to the case of a semi-infinite working section was later developed by Paquet [43], who specified boundary conditions for the streamwise velocity increment on an upstream measurement face.

---

[1] If these terms cannot be neglected then it will, in general, be necessary to determine the streamwise velocity increment and hence the perturbation potential at the measurement surface by integrating the Euler equations in the direction of the tunnel axis (Ashill and Keating [2] and Maarsingh et al [34]).

Methods using either the wall interference potential or the streamwise velocity increment are 'autocorrective'. This means that calculations by them of corrected stream speed are automatically compensated for errors in the reference-pressure measurement (Capelier et al [7] and Paquet [43]).

4.1.2.2 NEUMANN PROBLEM

For the Neumann problem the normal gradient of the interference potential, or the normal component of the wall-induced velocity, is given on the boundary. The required Green's function, G_N, is one with vanishing normal gradient on S giving

$$4\pi \varphi_I(P) = - \int_S \left(\frac{\partial \varphi}{\partial n} - \frac{\partial \varphi_F}{\partial n} \right) G_N \, dS. \qquad (4.8)$$

The term $\partial\varphi/\partial n$ in Equation (4.8), implies that the normal component of velocity or the flow angle has to be specified on S. The measurement of flow angle causes no significant problems for wind tunnels with solid, though possibly, flexible walls, since the flow angle is essentially defined by the condition of no flow through the walls[2]. On the other hand, for porous or slotted walls, flow angle needs either to be measured or to be deduced from wall and plenum pressure measurements by using elaborate theoretical models. Measurement of flow angle with the required accuracy is extremely difficult. For this reason, methods of the 'Neumann' type are not favoured for porous or slotted-wall wind tunnels. Indeed, the use of the wall-induced streamwise velocity as a boundary condition, was originally proposed by Capelier et al [7] with just this problem in mind.

Where the difference in normal velocity is used as the boundary condition, as for Equation (4.8), the technique is autocorrective in that errors in measurements of normal velocity or flow angle far upstream of the model are compensated for by the method.

4.1.2.3 MIXED PROBLEM

In some cases, where the normal velocity is well defined on parts of the boundary and the streamwise velocity increment or the perturbation potential on other parts, a mixture of types of boundary condition may be appropriate. An example of where such a treatment might be used is for a case with solid sidewalls and upper and lower walls that are either perforated, slotted or flexible. In such cases, the boundary S_T may be divided into S_1 and S_2, on which conditions of the 'Dirichlet' and 'Neumann' types are, respectively, applied. If, for example, the upstream and downstream faces are sufficiently remote from the model for their effects to be ignored, the solution for the interference potential may be expressed as:

$$4\pi \varphi_I(P) = \int_{S_1} (\varphi - \varphi_F) \frac{\partial G_{DN}}{\partial n} \, dS - \int_{S_2} \left(\frac{\partial \varphi}{\partial n} - \frac{\partial \varphi_F}{\partial n} \right) G_{DN} \, dS, \qquad (4.9)$$

to be cylindrical and of infinite length; the wall-interference potential, φ_I, was expressed as the sum of contributions due, respectively, to the model, an infinite array of images of the model simulating the solid sidewalls and a remainder to allow for the flexible roof and floor. The last contribution was determined by separation of variables and Fourier transforms of the resulting set of two-dimensional, partial-differential equations. Smith [47],[49] used mixed boundary conditions in his treatment, by a panel method, of wall

---

[2] It may be necessary to allow for the effect on normal velocity at the measurement surface of the change in wall boundary layer displacement thickness between the empty tunnel and the model-in-tunnel cases (see Chapter 4.2).

interference on the flow over two-dimensional aerofoils in a working section that was slotted in one part and solid upstream and downstream of it. Boundary pressures were measured only over a part of the working section, which extended beyond the slotted region. He applied conditions of the 'Dirichlet' type to this part (S_1) and 'Neumann' type conditions to the solid regions upstream and downstream of it (S_2).

Mokry et al [39] noted that some care needs to be taken with mixed boundary conditions at any line or point where the conditions change from one sort to another. They also raised concerns about the uniqueness of the solution which, in the case considered by Smith [47], is presumably ensured by satisfying the condition of smooth flow at the two joins.

4.1.2.4 MODEL REPRESENTATION ERRORS

As noted in Section 2.1 one-variable methods require some form of model representation. In principle, the simulation may be achieved with suitable distributions of potential singularities so long as the flow is subcritical at the tunnel walls. The problem is to determine the strengths of the singularities. Smith [47] noted the importance of accurate model representation, arguing that errors caused by inaccurate modelling could be as large as the interference quantity itself. For subcritical flows over wings or bodies at low angles of incidence, linear theory can be used with allowance for model thickness or cross-sectional area (Garner et al [15]) and with other modifications, as described below. However, for transonic flows or for flows with large regions of separation, the problem is much less easily solved owing to the non-linear character of the flow in the near field of the model. Numerical methods have been developed, in which various approximations to the Navier-Stokes equations have been solved for aerofoils and wing-body configurations (Kemp [23], Newman et al [42] and Rizk and Smithmeyer [45]). These methods require both the wind tunnel and 'free-air' flows to be calculated and are expected to be of particular value when there are supercritical-flow patches at the wall, but it is unlikely that it will be possible to correct such flows to 'free-air' conditions except in adaptive-wall tunnels (see Chapter 4.1.4). It would appear that these methods have not been used to calculate the strengths of the equivalent potential-flow singularities. However, Mokry [41], applying a suitable contour integration to numerical coupled solutions of the Euler and boundary-layer equations, has determined doublet strength for transonic flows over aerofoils with supercritical flows contained within the working section.

If numerical calculations of transonic flows, or, indeed, any other complex flows, are to be avoided, three possible approaches may be used to minimise errors due to model representation:

i) **Exploit an observed tendency for different types of boundary condition to have different levels of sensitivity to model representation errors.**

It may be noted that the contribution of the model representation term to the wall interference potential can be determined for each type of boundary condition by setting $\varphi = 0$ in Equation (4.6) and $\partial\varphi/\partial n = 0$ in Equation (4.8), while, for Equation (4.9), it follows by setting $\varphi = 0$ on S_1 and $\partial\varphi/\partial n = 0$ on S_2. This implies that, for wind tunnels with long, cylindrical working sections, the respective contributions due to model representation in methods of the 'Dirichlet' and 'Neumann' type can be inferred from classical results for tunnels with open-jet and solid walls and, for mixed boundary conditions, by a combination of wall types. In this respect, it is useful to think of a wind tunnel having a working section with the same cross section as the measurement surface and with classical wall boundary conditions, hereafter referred to as the 'equivalent wind tunnel'.

The observations in the last paragraph are not merely of academic interest, since they allow extensive experience with classical wall-interference methods to be used to assess the contribution to wall-induced velocities from imperfect model representation. In the past, particular emphasis has been placed on determining the strength of the doublet representing the volume effect of the model and its associated supercritical flow in the far field. The reason for this is that non-linear effects of compressibility affect doublet strength in a way that is not represented in linear theory, and, consequently, this is a possible source of error. It is therefore interesting to compare the wall corrections associated with a source-sink doublet placed on the tunnel axis in various equivalent wind tunnels of rectangular cross section. Results for the wall shape factor for the doublet

$$T = \frac{(BH)^{\frac{3}{2}}}{V}\,\frac{u_I{}^m}{U_F}$$

are plotted in Figure 4.3 against (effective) working section breadth to height ratio B/H, where $u_I{}^m$ is the wall-induced or blockage increment in streamwise velocity at the model for incompressible-flow conditions and V is model volume.

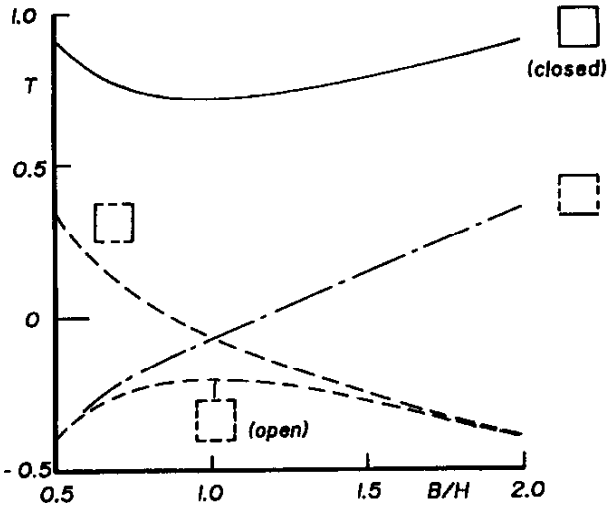

Fig 4.3 Wall shape factor T

Shown in the figure are cases with working sections that are **i)** fully-closed (Neumann), **ii)** fully-open (Dirichlet), **iii)** mixed, open sidewall and closed roof and floor and **iv)** mixed, open roof and floor and closed sidewalls. Results for the fully-closed and fully-open cases have been gleaned from information given by Garner et al [15], while the results for the two 'mixed' cases have been calculated for this study. For values of B/H close to unity, the 'Dirichlet' case gives a wall shape factor that is only 28% of the magnitude of that of the 'Neumann' approach, indicating that the 'Dirichlet' approach is to be preferred to the 'Neumann' approach from the point of view of minimising model-representation errors. For B/H = 1 the 'mixed' approach gives an even lower value, with a magnitude of only 10% of that of the 'Neumann' value. The 'mixed' approach also yields zero blockage (due to model representation) for mixed conditions of type iii) above with B/H = 1.17 or of type iv) with B/H = 1/1.17 = 0.85. These are significant results which could have an important bearing on where and how to apply wall boundary conditions with one-variable methods and possibly also on the design of any future wind tunnels.

Similar conclusions have been reached in calculations performed for 'long' bodies simulated by an axial distribution of sources or sinks, results of which are given by Ashill (1994), who presents a fuller account of a study of effects of types of boundary conditions on model representation errors.

It should be remembered that the porous or slotted region does not necessarily occupy the whole length of the working section. It may, therefore, be possible to exploit this feature by using, as Smith [47],[49] has done, boundary conditions which differ from one part of the working section length to another. It may be possible to decrease the open-area ratio of the equivalent wind tunnel by applying 'Neumann' type conditions where the wall is solid upstream (and downstream) of the slotted or perforated region. For slotted-wall tunnels, it may be possible to apply the solid-wall condition on parts of the slats between the slots to reduce the sensitivity to model representation errors. Kemp [22] applied boundary conditions in this way in his method for

three-dimensional models in a slotted-wall tunnel, but for the different reason that he was limited by the number of slat pressure measurements that were available.

Results for lift-interference parameters of a 'small' wing are shown in Figure 4.4 for various types of classical boundary conditions (Garner et al [15]). For a square tunnel the smallest values of the classical parameters δ_0 and δ_1 are obtained with the walls of the equivalent wind tunnel open at the sides and closed in the roof and floor, for which $\delta_0 = 0$. This means that, if an accurate estimate of lift interference is the overriding consideration and there are doubts about the accuracy of the representation of the model lift distribution, 'Dirichlet' type conditions should be applied at the sidewalls and 'Neumann' type conditions at the roof and floor. Plainly, this is an unattractive option for tunnels with a slotted roof and floor such as ETW and NTF. Fortunately, the lift distribution of models is usually determined from measurement or can be estimated with some confidence. Consequently, errors from this source are unlikely to be serious.

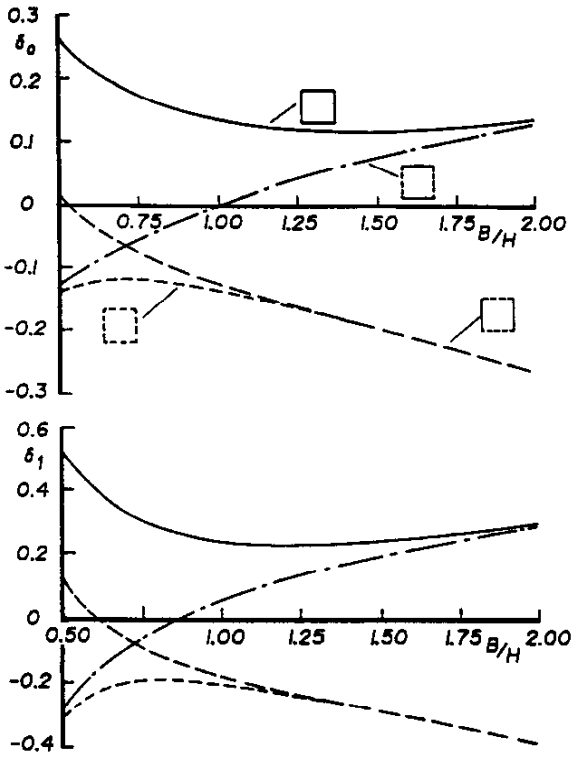

Fig 4.4 Lift interference for 'small' wings on axis of equivalent wind tunnel of rectangular cross section

Basing his ideas on the earlier work of Davis [11], Schairer [46] developed a method for two-dimensional tests in which the influence of model representation was eliminated altogether by using measurements of one flow variable, normal velocity, at two separate surfaces. Schairer found that he was unable to obtain wall-induced velocities of adequate accuracy owing to the limited range of the measurements along the working section. The method does not seem to have been adapted to three-dimensions, but studies by Davis [11] suggest that the method is much more complicated for three-dimensional flows.

ii) Make use of experience from testing in solid-wall wind tunnels.

Evans [12] was able to make significant progress using measurements of wall pressures. As well as drawing attention to the importance of representing body length for typical models, he showed the significance of using the corrected Mach number in the Prandtl-Glauert factor when determining the strengths of the sources and sinks representing a body. This important point, which does not appear to have been fully grasped in some later work, is illustrated in Figure 4.5 showing comparisons between calculation and measurement of wall pressure measurements in the RAE 10ft x 7ft Tunnel for a series of bodies. Since the correction is not known *a priori*, this implies an iteration process. However, if, as is often the case, the corrections are calculated 'on line' during the test, the nominal Mach number can be adjusted until the corrected Mach number corresponds with the desired value. Evans concluded that an error in the solid blockage at drag-rise conditions could be reconciled with an increase in the effective volume of the model, and he suggested that this error is directly proportional to the rise in drag coefficient.. Although plausible and based on comparisons with wall pressure measurements, this result does not have a rigorous theoretical basis.

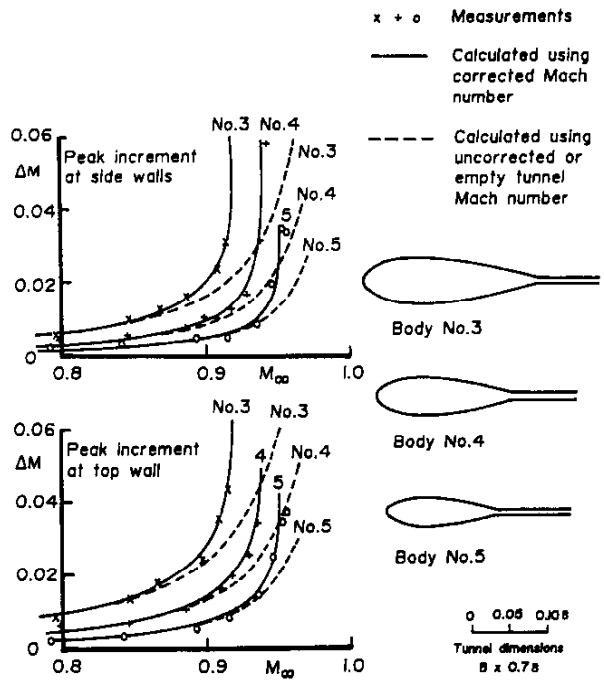

Fig. 4.5 Comparison of measured and calculated peak increments in wall Mach numbers for three bodies after Evans (1949)

iii) Obtain more accurate estimates of singularity strengths using asymptotic expansion or other approximate methods.

Using the method of matched asymptotic expansions, Chan [8],[9] established a correction for compressible non-linear effects to doublet strength for two-dimensional aerofoils. For the same problem, Smith [48] used Green's formula to obtain an estimate of the doublet strength. Mokry [41] showed that doublet strength depends on aerofoil camber and angle of incidence as well as thickness. It would appear that these approaches have not yet been extended to three dimensions. No correction is needed to vortex strength for compressibility if the spanwise distribution of local lift coefficient of a wing is known either from pressure measurements or can be inferred from overall-force measurements.

4.1.3 WALL-SIGNATURE METHODS

As noted earlier, there are two variants of the wall-signature method. In the first, one component of velocity is known and the other is measured at a limited number of points on the measurement boundary. By matching calculation to measurement at this boundary it is then possible to determine the strengths of the singularities representing the model. The best known application of this type of method is to solid-wall wind tunnels, for which the normal-velocity component may be taken to be zero at the walls. Therefore, with the measurement boundary taken to coincide with the walls, the solution to the Neumann problem, Equation (4.8), may be used to obtain:

$$4\pi\varphi_I(P) = -\int_S \frac{\partial\varphi_F}{\partial n} G_N \, dS. \qquad (4.10)$$

After differentiation by X, Equation (4.10) may be re-expressed as:

$$4\pi[u(P) - u_F(P)] = -\int_S \frac{\partial\varphi_F}{\partial n} \frac{\partial G_N}{\partial X} \, dS,$$

or as

$$u(P) = u_F(P) - \frac{1}{4\pi}\int_S \frac{\partial\varphi_F}{\partial n}\frac{\partial G_N}{\partial X} \, dS. \qquad (4.11)$$

Here the differentiation with respect to X has been taken under the integral sign because G_N is smooth and continuous within the region of integration. If the point P is taken to be limitingly close to the walls, the left-hand side of Equation (4.11) may then be defined by static-pressure measurements at the walls, together

with the linear Bernoulli Equation (4.6), at N points. Thus, if the model is represented by a distribution of N singularities, Equation (4.11) may be regarded as a linear (integral) equation for the unknown .singularity strengths. For a wind tunnel with a cylindrical working section of length that is sufficiently large to be assumed infinite, the integral in Equation (4.11) may be replaced by a doubly-infinite sum for each singularity, representing the image effect of the tunnel walls.

The idea behind this approach, which is illustrated in Figure 4.6, goes back to the 1940's when the problems of testing at high subsonic speed in solid-wall tunnels were first addressed. Mokry et al [39], reviewing various early methods for two-dimensional flows, described a simple procedure to determine the strengths of a doublet, vortex and source representing a lifting aerofoil from static-pressure measurements at three points on both the roof and floor of the working section. They argued that methods of this type are superseded by two-variable methods, to be described later, which need no model representation. A contrary view is that wall-signature methods are to be preferred in some applications because they need relatively-few measurement points compared with two-variable methods. Smith [47], using a method similar to that described by Mokry [37], suggested that an aerofoil with a chord to working section height ratio of about 0.2 could probably be represented adequately in the far field by about ten singularities placed at a single point, requiring ten measurement points. Evans [12] found that it was possible to represent a body of revolution by a point source and point sink, in each case placed at a fixed distance from the centre of volume of the body on its axis, indicating the need for two measurement points. These numbers of measurement points would be considered much too low for a two-variable method. However, where the model flow field is complex and not easily represented by singularities, two variable methods are probably to be preferred (see Section 4.2.4). Nevertheless, the wall-signature strategy has been used to determine wall corrections for models with separated flows (Hackett and Wilsden [18], [19] and Hackett et al [20]) and jets in cross flow (Wilsden and Hackett [52]).

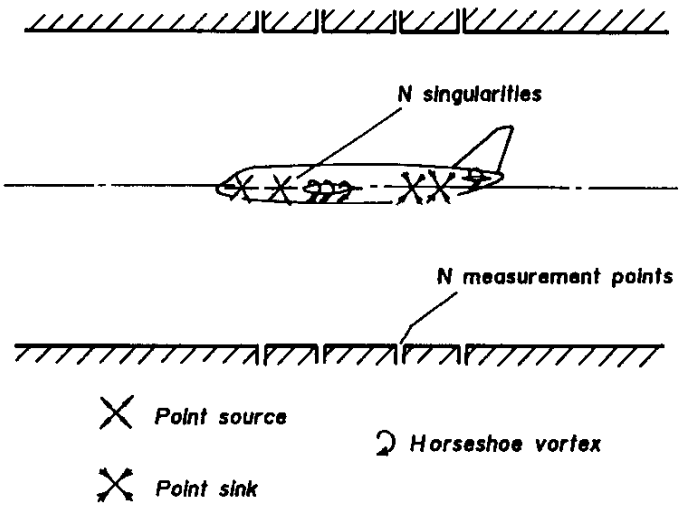

Fig 4.6 Sketch illustrating 'Wall signature method" for solid wall wind tunnels

Le Sant and Bouvier [29] found that the matrix inversion needed to solve equation (4.11) is ill-conditioned owing to the insensitivity of the flow at the walls to details of the model. They suggested that this problem could be overcome by gathering singularities into groups with fixed relative strengths. A method similar to this is routinely used to determine the blockage for tests at subsonic speeds in the 8ft x 8ft (solid-wall) Wind Tunnel at the Defence Evaluation and Research Agency (DERA), Bedford (Isaacs [21]). The axial source distribution representing model volume is assumed to be represented adequately by linear theory and the theory is used merely to determine the ratio between the mean value of the streamwise velocity increment at four points on the walls (two on the roof and two corresponding ones on the floor) and the blockage increment at a reference point on the model. Measurements of the change in static pressure coefficient between the empty tunnel case and the case with the model in the wind tunnel at these same points provide sufficient

information to determine the blockage at the model reference point. Experience has suggested that the method is reliable (Isaacs [21]).

If comprehensive measurements could be made of static pressures at the measurement boundary, a similar procedure to that described above could, in principle, be developed using, instead, the 'Dirichlet' approach, together with limited measurements of flow angle to give normal velocity at the boundary. This approach may be useful for wind tunnels with perforated or slotted walls but it has not yet been tried as far as is known.

The second variant of the method uses a 'wall' pressure signature to establish or check the value or values of a parameter linking the flow variables at the measurement surface. This approach has been used by Vaucheret [50], who combined a validated model representation with wall pressure measurements, to infer the porosity of the roof and floor liners of the ONERA S2Ma Tunnel. In a similar way, Goldhammer and Steinle [16] made static pressure measurements on four rails to verify the porosity factor used in a simulation of slotted walls. As with Vaucheret's method, a model representation is used.

4.1.4 TWO-VARIABLE METHODS

In section 4.1.2.4 it was shown that the contribution of the model representation term to a particular component of wall-induced velocity at a point on the model could be eliminated by a suitable mixture of types of boundary condition on S. Equation (4.5) indicates that the contribution of model representation terms vanishes identically when

$$0 = \int_S \left(\frac{\partial \varphi_F}{\partial n} G - \varphi_F \frac{\partial G}{\partial n} \right) dS. \tag{4.12}$$

This suggests that the Green's function satisfying this condition is that for an interference-free, equivalent wind tunnel. In turn, this suggests that the appropriate Green's function is:

$$G = G_F = \frac{1}{r},$$

the free-space Green's function (Mokry et al, [39]), which, in aerodynamic terms, may perhaps be called the 'free-air' Green's function. For this Green's function, Green's formula gives

$$\int_S \left(\frac{\partial \varphi_F}{\partial n} \frac{1}{r} - \varphi_F \frac{\partial}{\partial n} \left(\frac{1}{r} \right) \right) dS - \int_{V_0} \frac{1}{r} \Delta^2 \varphi_F \, dV = 0, \tag{4.13}$$

where V_0 refers to volume integration in the fictitious region, R, outside the measurement region (Fig 4.1). Thus, provided that the perturbations in the free-air flow outside the working section are 'small', the perturbation potential φ_F may be considered harmonic in this region with the consequence that

$$\int_S \left(\frac{\partial \varphi_F}{\partial n} \frac{1}{r} - \varphi_F \frac{\partial}{\partial n} \left(\frac{1}{r} \right) \right) dS = 0.$$

Thus, for flows of this type, the Green's function G_F satisfies equation (4.12) to give, in place of equation (4.5), an expression no longer containing model-related terms

$$4\pi \varphi_I(P) = - \int_S \left(\frac{\partial \varphi}{\partial n} \frac{1}{r} - \varphi \frac{\partial}{\partial n} \left(\frac{1}{r} \right) \right) dS. \tag{4.14}$$

This expression was derived by Ashill and Weeks [4] in a somewhat different way to the way presented here and it appears in a number of references (Kraft [25], Mokry [35] and Labrujere [28]) giving a particularly elegant derivation. Corresponding expressions have been obtained for plane, two-dimensional flows, using, variously, Fourier transforms (Lo [33]), Green's formula in the plane (Ashill and Weeks [5] and Labrujere [28] and Cauchy's integral formula (Ashill and Weeks [5], Kraft and Dahm [26] and Smith [49]).

A consequence of not having to know anything about the flow around the model is that it is necessary to measure both components of velocity at all parts of the measurement boundary. The first term under the integral sign in equation (4.14), recognised as the contribution of sources of strength $\partial\varphi/\partial n$, requires the normal component to be known at S, while, for the second term, which is the contribution of source doublets, the streamwise velocity increment on S is needed. For solid-wall tunnels, including certain types of adaptive-wall wind tunnels with flexible liners, this poses no significant problems, since the normal component is effectively defined by the condition of no flow through the walls[3]. For other types of walls, however, the measurement of normal velocity over the whole measurement boundary is much more difficult. As a result, the method has largely been restricted, up to now, to solid-wall tunnels (Ashill and Weeks [4] and Ashill and Keating [2], [3]), although some progress is being made in determining the normal component in perforated and slotted wall tunnels (Freestone and Mohan [13] and Mohan and Freestone [14]).

A major enhancement that became possible with two-variable methods is the calculation of wall interference for complex flows in solid-wall tunnels, e.g. those for high-lift configurations, helicopters and other V/STOL aircraft. The facility to ignore the flow around the model is an important advantage. One area which has been known to cause difficulties in the past is the calculation of blockage for aircraft configurations at high angles of attack, where the flow over the lifting surface is partially separated. In particular, experience in various establishments with the semi-empirical method due to Maskell for calculating blockage was not entirely favourable. However, it was found that, in many cases, Maskell's method gives an overestimate for blockage correction with a consequential underestimate in maximum lift coefficient. This view was confirmed for a combat-aircraft configuration (Ashill and Keating [2], [3]) and for a civil transport model (Kirkpatrick and Woodward [24]) by comparisons between results from Maskell's method and of calculations using a two-variable method. A careful and thorough assessment of a two-variable method for tests at low speed and high lift has been made by Maarsingh et al [34].

Another area where two-variable methods have been used is in the calculation of residual wall interference in adaptive-wall tunnels (Lewis et al [32] and Lewis [31]), where, as noted before, it is routinely necessary to measure both flow angle and static pressure at the measurement boundary. Mokry [35] showed how equation (4.14) may be manipulated to give a convergence formula to allow the shape of the of the walls of an adaptive-wall wind tunnel to be altered in one step to give nominally interference-free flow. He also showed that two-variable methods are autocorrective in character.

Since the Green's function in equation (4.14) is known, special techniques for determining the function, or equivalent techniques, are unnecessary in two-variable methods. Methods of this type can, therefore, be applied to measurement boundaries of irregular shape with relative ease. In this respect, two-variable methods may be favourably contrasted with one-variable methods.

If the free-air perturbation potential in the fictitious region R is not harmonic, then the volume integral in equation (4.13) can no longer be ignored and equation (4.14) is replaced by

[3] As noted before, allowance may need to be made for the change in wall boundary-layer thickness between the tunnel empty and model-in-tunnel cases, further information being given in Chapter 4.2.

$$4\pi\varphi_I(P) = -\int_S \left(\frac{\partial\varphi}{\partial n}\frac{1}{r} - \varphi \frac{\partial}{\partial n}\left(\frac{1}{r}\right) \right) dS + \int_{V_o} \left(\frac{1}{r}\right) \Delta^2\varphi \, dV. \qquad (4.15)$$

It may be thought that this is an extreme situation and, as mentioned before, that it would not be possible to correct such flows to equivalent free-air conditions. However, flows of this type are found in adaptive-wall tunnels at high subsonic speeds (Lewis et al [32] and Lewis [30]), and it has therefore been necessary to establish the magnitude of the residual corrections for wall constraint (Lewis [30]). For practical reasons, it might be convenient to avoid eliminating tunnel-wall interference altogether in adaptive-wall wind tunnels, concentrating, instead, on ensuring that the wind-tunnel flow may be corrected to equivalent free-air conditions.

A problem with equation (4.15) is that it requires the source term or volume integral in the fictitious region R outside the measurement region to be calculated. This requires a (transonic) flow-field calculation as well as the evaluation of the integral. To avoid the latter difficulty it is useful to think of a flow in the fictitious region R with a velocity potential Φ_R that is identical to the free-air flow velocity potential in the near field of the model. This implies that the difference in perturbation potentials ($\varphi_F - \varphi_R$) is harmonic in this region. Thus, if Green's formula is applied to the perturbation potential φ_R in the same way as was done to obtain equation (4.13) and the resulting expression is combined with equation (4.15), it is found that

$$4\pi\varphi_I(P) = -\int_S \left(\left(\frac{\partial\varphi}{\partial n} - \frac{\partial\varphi_R}{\partial n} \right) - (\varphi - \varphi_R) \frac{\partial}{\partial n}\left(\frac{1}{r}\right) \right) dS + \int_{V_o} \left(\frac{1}{r}\right) \Delta^2(\varphi_F - \varphi_R) \, dV,$$

$$= -\int_S \left(\left(\frac{\partial\varphi}{\partial n} - \frac{\partial\varphi_R}{\partial n} \right) \frac{1}{r} - (\varphi - \varphi_R) \frac{\partial}{\partial n}\left(\frac{1}{r}\right) \right) dS. \qquad (4.16)$$

Mokry [35] refers to this variant of the two-variable approach as an 'interface - discontinuity method', expressing the fact that the equation contains discontinuities in the normal velocity and perturbation potential across the measurement boundary.

For a solid-wall tunnel

$$\frac{\partial\varphi_R}{\partial n} = \frac{\partial\varphi}{\partial n},$$

and thus equation (4.16) reduces to

$$\varphi_I(P) = \frac{1}{4\pi} \int_S (\varphi - \varphi_R) \frac{\partial}{\partial n}\left(\frac{1}{r}\right) dS.$$

This expression is recognised as the potential at P due to a distribution of source doublets of strength ($\varphi - \varphi_R$) on S, and, for a cylindrical measurement surface, the integral may be rewritten in terms of a distribution of horseshoe vortices (Ashill and Keating [3] and Mokry [35]). The strength of each of these vortices is directly proportional to the local wall loading. Judd (unpublished research, Southampton University) derived the corresponding expression for two-dimensional flows which was used by Goodyer and Wolf [17] to determine residual corrections in the flexible-wall tunnel at Southampton University. This method was later extended to three dimensions by the Southampton-University group (Lewis [31]). For the study of aerofoils at transonic speeds in the same wind tunnel, Lewis [30] performed calculations of the fictitious flow (effectively to determine either φ_R or $\partial\varphi_R/\partial x$) using a transonic small-perturbation method. Since the boundaries of the fictitious flow are cylindrical or planar, this calculation is less demanding than that for the free-air flow about the model at transonic speeds, particularly in three dimensions.

If the external flow is solved as a Dirichlet problem so that

$$\varphi_R = \varphi$$

at the measurement surface, equation (4.16) reduces to

$$\varphi_I(P) = -\frac{1}{4\pi} \int_S \left(\frac{\partial \varphi}{\partial n} - \frac{\partial \varphi_R}{\partial n} \right) \frac{1}{r} dS,$$

which is the potential due to a distribution of sources of strength ($\partial\varphi/\partial n - \partial\varphi_R/\partial n$). This approach was suggested by Rebstock and Lee [44].

REFERENCES to Chapter 4.1

[1] Ashill, P. R., 1993, "Boundary-flow measurement methods for wall interference assessment and correction - classification and review." AGARD-CP-335, pp 1.1 - 1.12.

[2] Ashill, P.R. and Keating, R.F.A., 1985, "Calculation of tunnel wall interference from wall-pressure measurements." RAE TR 85086,. (This report provides a more detailed account of the work referred to in the following reference).

[3] Ashill, P.R. and Keating, R.F.A., 1988, "Calculation of tunnel wall interference from wall-pressure measurements." Aeronautical Journal, Vol. 92, No.911, pp.36-53.

[4] Ashill, P.R. and Weeks, D.J., 1982, "A method for determining wall-interference corrections in solid-wall tunnels from measurements of static pressure at the walls." AGARD-CP-335, pp.1.1-1.12.

[5] Ashill, P.R. and Weeks, D.J., 1978 , "An experimental investigation of the drag of thick supercritical aerofoils - a progress report." RAE TM Aero 1765.

[6] Ashill, P.R. and Weeks, D.J., 1981, "Techniques developed in Europe for tunnel-wall corrections using measured boundary conditions." Unpublished Proceedings of the 1981 AGARD FDP Subcommittee on Wind Tunnels and Testing Techniques Meeting on 'Integration of Computers and Wind Tunnel Testing', RAE Bedford UK, 18-19 February. 1981

[7] Capelier, C., Chevallier, J.P. and Bouniol, F., 1978, "Nouvelle methode de correction des effets de parois en courant plan." La Recherche Aerospatiale, 1978-1.

[8] Chan, Y.Y., 1980, "A singular perturbation analysis of two-dimensional wind tunnel interferences." Journal of Applied Mathematics & Physics, Vol. 31, pp.605-619.

[9] Chan, Y.Y., 1980, "Lift effect on transonic wind tunnel blockage." Journal of Aircraft, Vol. 17, No.12, pp.915-916.

[10] Chevallier, J.P., 1983, "Survey of ONERA activities on adaptive-wall applications and computation of residual corrections." NASA CP-2319, pp.43-58.

[11] Davis, S.S., 1981, "A compatibility assessment method for adaptive-wall wind tunnels." AIAA Journal, Vol. 19, No. 9, pp.1169-1173.

[12] Evans, J.Y.G., 1949,"Corrections to velocity for wall constraint in any 10 x 7 rectangular subsonic wind tunnel." ARC R&M 2662.

[13] Freestone, M. M. and Mohan, S. R., 1994, „Interference determination for wind tunnels with slotted walls.", AGARD-CP-535, pp 19-1 - 19-12.

[14] Mohan, S. R. and Freestone, M. M., 1994, „Interference determination for three dimensional flows in slotted liner wind tunnels." ICAS-94-3.3.1, Anaheim, California, USA, 18-23 Sept. 1994

[15] Garner, H.C., Rogers, E.W.E., Acum, W.E.A. and Maskell, E.C., 1966, "Subsonic wind tunnel wall corrections.", AGARD-AG-109.

[16] Goldhammer, M.I. and Steinle, F.W., 1990, "Design and validation of advanced transonic wings using CFD and very high Reynolds number wind tunnel testing." ICAS 90-26.2.

[17] Goodyer, M.J. and Wolf, S.W.D., 1980, "The development of a self-streamlining flexible walled transonic test section." USA AIAA-80-440-CP.

[18] Hackett, J.E. and Wilsden, D.J., 1975, "Determination of low speed wake-blockage corrections via tunnel-wall static pressure measurements." AGARD-CP-174, pp.22.1-22.9.

[19] Hackett, J.E. and Wilsden, D.J., 1979, "Estimation of tunnel blockage from wall pressure signatures: a review and data correlation." NASA CR-152241.

[20] Hackett, J.E., Wilsden, D.J., and Stevens, W.A., 1981, "A review of the wall pressure signature and other tunnel constraint correction methods for high angle-of-attack tests." AGARD-R-692.

[21] Isaacs, D., 1969, "Calibration of the RAE Bedford 8ft x 8ft wind tunnel at subsonic speeds, including a discussion of the correction to the measured pressure distribution to allow for the direct and blockage effects due to the calibration probe." ARC R&M 2777.

[22] Kemp, W.B. Jr., 1988, "A panel method procedure for interference assessment in slotted-wall wind tunnels." USA AIAA-88-2537.

[23] Kemp, W.B. Jr., 1976, "Towards the correctable-interference transonic wind tunnel." Proceedings of the AIAA 9th Aerodynamic Testing Conference, 7-9 June 1976, pp.31-38.

[24] Kirkpatrick, D.L.I. and Woodward, D.S., 1990, "Priorities for high-lift testing in the 1990s." AIAA-90-1413.

[25] Kraft, E.M., 1983, "An overview of approaches and issues for wall interference assessment/correction." NASA CP-2319, pp.3-20.

[26] Kraft, E.M. and Dahm, W.J.A., 1982, "Direct assessment of wall interference in a two-dimensional subsonic wind tunnel." USA AIAA-82-0187.

[27] Küchemann, D., 1978, "The aerodynamic design of aircraft." London, Pergamon Press.

[28] Labrujere, Th. E., 1984, "Correction for wall interference by means of a measured-boundary-condition method." Holland NLR TR 84114 U.

[29] Le Sant, Y., and Bouvier, F., 1992, "A new adaptive test section at ONERA Chalais-Meudon." Proceedings of European Forum on Wind Tunnels and Wind Tunnel Test Techniques, Southampton University, 14-17 September 1992, Paper 41.

[30] Lewis, M.C., 1988, "Aerofoil testing in a self-streamlining flexible walled wind tunnel." NASA CR-4128.

[31] Lewis, M. C., 1991, "Two-dimensional wall adaptation for three-dimensional flows." Proceedings of the International Conference on Adaptive Wall Wind Tunnel Research and Wall-Interference Correction (ICAW), June, 1991, Paper A2.

[32] Lewis, M. C., Taylor N. J. and Goodyer, M. J., 1992, "Adaptive wall technology for three-dimensional models at high subsonic speeds and aerofoil testing through the speed of sound." Proceedings of the Royal Aeronautical Society Symposium 'Wind Tunnels & Wind Tunnel Test Techniques', Southampton University, 14-17 October 1992, Paper 32.

[33] Lo, C.F., 1978, "Tunnel interference assessment by boundary measurements." AIAA Journal, Vol. 16, No.4, pp.411-413.

[34] Maarsingh, R. A., Labrujere, Th. E., and Smith, J., 1988, "Accuracy of various wall-correction methods for 3D subsonic wind-tunnel testing." AGARD-CP-429, pp.17.1-17.13.

[35] Mokry, M., 1989, "Residual interference and wind tunnel wall adaptation." USA AIAA-89-0147.

[36] Mokry, M. and Ohman, L. H., 1980, "Application of the Fast Fourier Transform to two-dimensional wind tunnel wall interference." Journal of Aircraft, Vol. 17, No. 6, pp.402-408.

[37] Mokry, M., 1971, "Higher order theory of two-dimensional wall interference in a perforated wall wind tunnel." Canada NRC LR-853.

[38] Mokry, M., 1982, "Subsonic wall interference corrections for finite-length test sections using boundary pressure measurements." AGARD-CP-335, pp.10.1-10.15.

[39] Mokry, M., Chan, Y. Y., Jones, D.J. and Ohman, L. H. (ed.), 1983, " Two-dimensional wind tunnel wall interference." AGARD-AG-281.

[40] Mokry, M., Digney, J. R. and Poole, R. J. D., 1987, "Doublet-panel method for half-model wind-tunnel corrections." Journal of Aircraft, Vol. 24, No. 5, pp. 322-327.

[41] Mokry, M., 1995, „On the subsonic and transsonic doublet in the farfield representation of an airfoil", AIAA-95-1879

[42] Newman, P.A. Kemp, W. B. Jr. and Garriz, J. A., 1988, "Emerging technology for transonic wind-tunnel-wall interference assessment and corrections." USA SAE Paper 881454.

[43] Paquet, J. B., 1979, "Perturbations induites par les parois d'une soufflerie, methods integrals." These Doc.Ing., Universite de Lille.

[44] Rebstock, R. and Lee, E. E. Jr., 1988, "Capabilities of wind tunnels with two adaptive walls to minimize boundary interference in 3D model testing." Transonic Symposium: theory, application, and experiment, NASA Langley, April 1988, NASA CP-3020 Vol. 1, Part 1, pp.891-910, March 1989.

[45] Rizk, M.H. and Smithmeyer, M. G., 1982, "Wind tunnel wall interference corrections for three-dimensional flows." Journal of Aircraft, Vol. 19, No.6, pp.465-472.

[46] Schairer, E. T., 1984, "Two-dimensional wind-tunnel interference from measurements on two contours." Journal of Aircraft, Vol. 21, No.6, pp.414-419.

[47] Smith, J., 1981,"A method for determining 2D wall interference on an aerofoil from measured pressure distributions near the walls and on the model."Holland NLR TR 81816 U.

[48] Smith, J., 1986, "A transonic model representation for two-dimensional wall interference assessment." Holland NLR TR 86026 U.

[49] Smith, J., 1982, "Measured boundary condition methods for 2D flows." AGARD-CP-335, pp.9.1-9.15.

[50] Vaucheret, X., 1982, "Amelioration des calculs des effets de parois dans les souffleries industrielles de l'ONERA." AGARD-CP-335, pp.11.1-11.12, (English translation in NASA TM-76971).

[51] Weatherburn, C. E., 1978, "Advanced vector analysis." London, G.Bell & Sons Ltd.

[52] Wilsden, D. J. and Hackett, J. E., 1983, "Tunnel constraint for a jet in crossflow." NASA CP-2319, pp.273-290.

4.2 CLOSED TEST SECTIONS

LIST OF SYMBOLS for chapter 4.2

B working section breadth

C Working section cross-sectional area

D Hydraulic diameter

H working section height

M free-stream Mach number

N parameter defined by Adcock and Barnwell (1984)

S Model reference area

TOLC TOLerance for Columns

β Prandtl-Glauert factor, $\beta = \sqrt{(1-M^2)}$

Δ Increment due to presence of model

δ Lift interference parameter

δ^* Wall boundary layer displacement thickness in empty tunnel at model station

θ Wall boundary layer momentum thickness in empty tunnel at model station

Ω Ratio of solid blockage in a wind tunnel of given height to breadth ratio with wall boundary layers to the maximum value of solid blockage in the same wind tunnel without boundary layers

4.2.1 BACKGROUND

The possible benefits of using measurements of wall pressures to calculate wall-interference corrections in closed-wall test sections were realised in the early 1940's when compressibility effects on the flows over wings and bodies were first observed (Göthert [13], Thom [32]). A review of this early work is given in Section 5 of AGARDograph 109 by Garner et al [11]. It was appreciated early on that linear-theory descriptions of the near-field flow around the model are increasingly inadequate as free-stream Mach number increases towards unity. This led to the idea of using wall pressures to determine the strengths of the singularities representing the model. This was justified on the grounds that the flow satisfies the linearised potential equation in the far field. Methods of this type are known as wall-signature or wall pressure signature methods, the underlying theory for which has been described in Section 4.1.3.

In the 1970's an analogous problem was discovered with the representation of wind-tunnel models at high lift, in which flow separation may occur on part of the model (Hackett and Wilsden [14], [16], and Hackett, Wilsden and Stevens [17]). For flows of this type linear theory is totally inadequate for modelling the near field. Hackett and his colleagues used wall pressures to determine the strengths of singularities representing the model flow in the far field. This aspect is considered in more detail in Sections 4.2.5 and 4.2.6, and in Section 8.3. The usual Neumann condition of zero normal velocity at the walls was applied by using the classical method of images. Hackett's group was able to demonstrate the application of the wall signature method to a wide range of flows, including wings with jet flaps. A related approach has been adopted by Ulbrich, Lo and Steinle [33], Ulbrich and Steinle [34], [35].

The development of the two-variable method in the late 1970's provided a further technique for calculating wall interference in closed-wall tunnels. The derivation of this method has been given in Section 4.1.4

and in this approach wall interference is defined by the distributions of two flow variables on a surface surrounding the model - the streamwise and normal components of velocity. No model representation is needed. If the surface is taken to coincide with the wind-tunnel walls, the normal component is usually set to zero to satisfy the condition of no flow through the walls, as with the wall signature method. However, where there are significant interactions between the constrained flow over the model and the wall boundary layers, allowance may need to be made for the change in displacement effect of the wall boundary layers. This aspect is discussed further in Section 4.2.2. This leaves only one variable to be determined - the streamwise velocity - and this can be inferred from Bernoulli's equation so long as the velocity perturbations at the wall are small compared with free-stream speed. This question is considered further in Section 4.2.4.

4.2.2 Boundary Conditions

The assumption usually used in both the wall signature and two-variable methods that the normal component of velocity is zero at the walls is equivalent to neglecting the interaction between the inviscid flow-field and the wall boundary layers. The validity of this assumption needs to be carefully assessed in each case. At one extreme where the flow perturbations are small, as for example in low-speed flows over a model at low lift, the effect on the wall boundary layers can be demonstrated to be negligible by simple one-dimensional considerations. At the other extreme, where flow perturbations are 'large', the interaction cannot be ignored. Examples of the latter type include flows were shock waves reach the wall (Lewis, 1988) and where the wall boundary layer separates as a result of large adverse pressure gradients induced by high-lift models (see Section 8).

Berndt [7] appears to have been the first to draw attention to the effect on blockage and the choking Mach number of the interaction between the inviscid flow-field associated with the model and wall interference and the wall boundary layers. He used a simplified method to calculate the effect. More recently a theoretical method with some simplifications has been presented by Adcock and Barnwell [2] for tunnels of rectangular cross section. This method is based on approach of Pindzola and Lo [26] for slotted-wall tunnels to solve the boundary-value problem for the perturbation potential. The simplifications made include the neglect of the change in wall shear stress due to the presence of the model and the assumption that the transformed shape factor is unity. Both these assumptions are justified for the high Reynolds number conditions of wind tunnels. In addition it is assumed that, in the empty tunnel, δ^* and θ, the wall boundary-layer displacement and momentum thicknesses may both be taken constant and equal to the values at the model station. It is further supposed that the wall boundary layer is two-dimensional in character so that its development when the model is in the working section can be described by the Von Karman momentum integral equation. As well as studying the effect on blockage, Adcock and Barnwell also considered the extent to which lift interference is influenced. For this purpose they represented model volume by a source doublet and the lifting effect by a vortex doublet. For the analysis they found it convenient to define a parameter

$$N = \frac{1}{1 + \frac{2\delta^*}{B}\left(1 + \frac{\delta^* + \theta}{\beta^2 \delta^*}\right)} \tag{4.17}$$

Results for the ratio of the solid blockage in a wind tunnel of given height to breadth ratio with wall boundary layers to the maximum value of solid blockage in the same wind tunnel without wall boundary layers, Ω, and the lift interference factor δ are shown in Figure 4.7 and 4.8 for working sections with H/B = 1. Charts such as these and others given by Adcock and Barnwell provide a useful guide as to the likely magnitude of the effect both on blockage and on angle of incidence in the absence of wall-pressure measurements (see below). Adcock and Barnwell observed that, owing to linearisations in the method, results obtained with it should only be used for values of N down to about 2/3. For the typical values $2\delta^*/B$ = 0.01, δ^*/θ = 1.4 and M = 0.8, N = 0.95 and, it may be inferred from Figure 4.7, that the maximum value of Ω is 0.85. In other words, for this case, the maximum blockage is 85% of the value predicted by classical inviscid theory. Regarding the effect on lift interference, Figure 4.8 shows that, at the position of the doublet, the wall boundary layers only affect the streamwise gradient of wall-induced upwash, the gradient becoming less as the parameter N decreases.

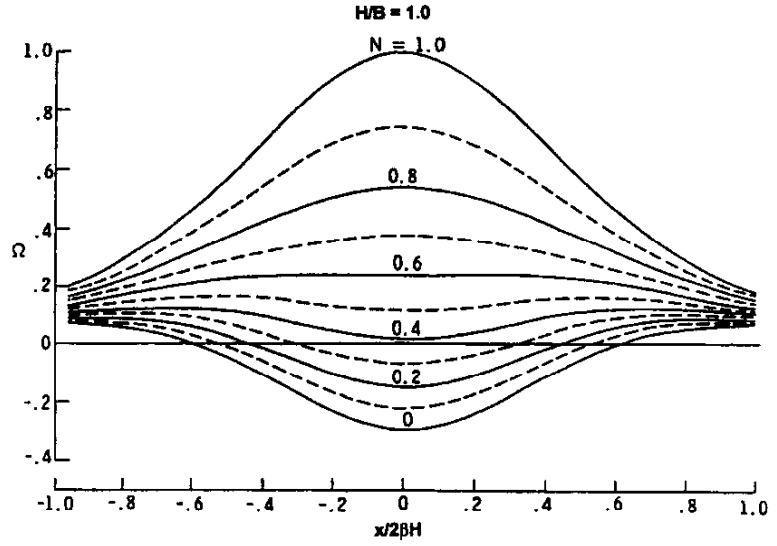

Figure 4.7 Calculated effect of wall boundary layers on blockage (after Adcock and Barnwell [2])

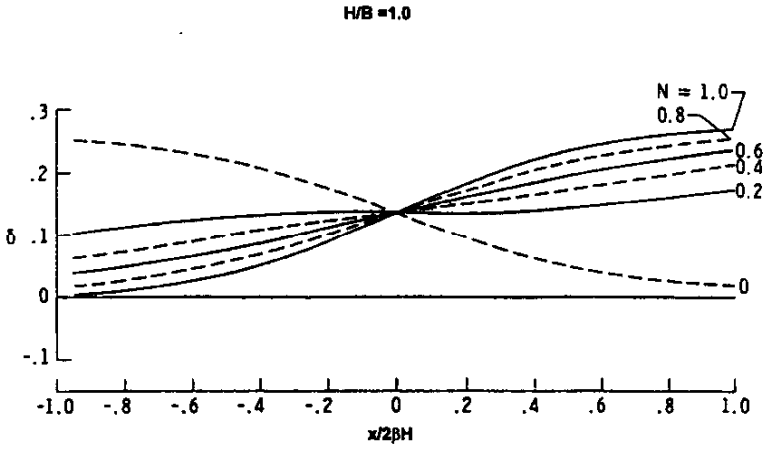

Figure 4.8 Calculated effect of wall boundary layers on lift interference (after Adcock and Barnwell, 1983)

A combined experimental-theoretical study has been made of the effect of wall boundary layers on the blockage of bodies at high subsonic speeds (Ashill, Taylor and Simmons [5]). Results for measured values of the mean of the increment in pressure coefficient, relative to empty-tunnel conditions, at the roof and floor of the working section for an axisymmetric body at zero angle of incidence are shown in Figure 4.9. In this figure the measured data are compared with results of a classical inviscid theory and those of the same theory but including allowance for the wall boundary-layer effect. The viscous theory gives improved agreement with measurement, particularly at the highest Mach number shown, M = 0.93. This theory differs from that due to Adcock and Barnwell in that a viscous-inviscid iteration process and a more-accurate form of the normal-velocity condition are used. As in the treatment of Adcock and Barnwell, Ashill et al solved the Von Karman momentum equation and, to simplify the boundary-value

problem, took the normal velocity to be constant around the working section at a fixed streamwise or axial station[1]. Furthermore, based on assessments of calculations of two-dimensional boundary layers by the method of Green, Weeks and Brooman (1973), they took the boundary-layer shape parameter to be a constant. With these assumptions the expression corresponding to equation (4.17) is:

$$N = \frac{1}{1 + \frac{2\delta^*}{B}\left(\frac{\delta^* + \theta}{\beta^2 \theta}\right)} \qquad (4.18)$$

Equations (4.17) and (4.18) give results for N that become increasingly close as Mach number and shape parameter δ^*/θ both tend to unity.

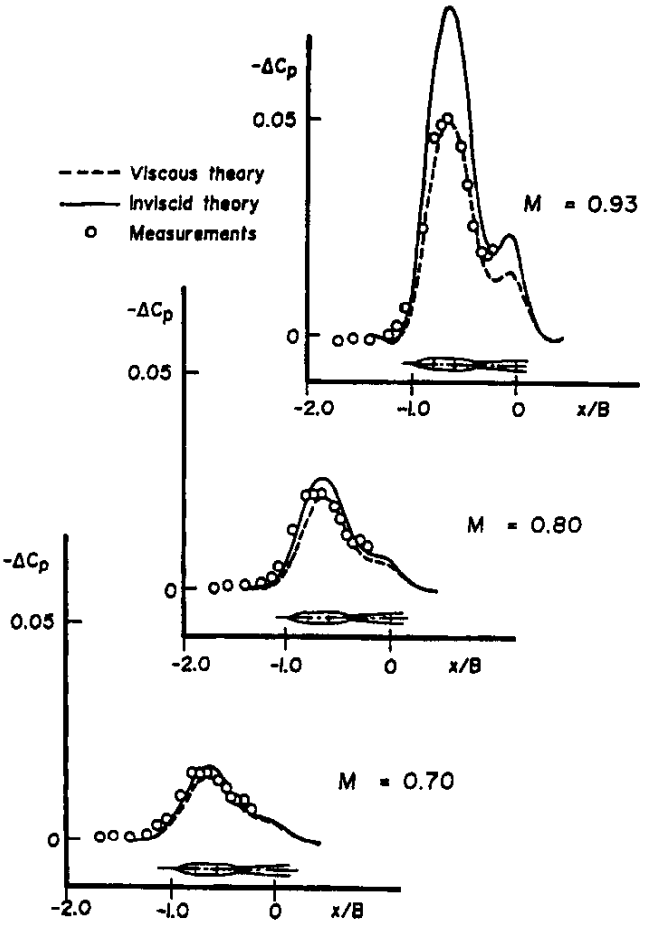

Figure 4.9 : Axial distributions of increment in wall static pressure coefficient due to the presence of the model : comparison between measurement and viscous and inviscid theories

Similar values for the change in blockage due to the wall boundary layers are obtained by the two methods. Figure 4.9 shows that the effect of the interaction is significant. Fortunately, methods that make use of wall-pressure measurements, such as those referred to above, account for a major part of the effect. This remark is supported by the results of calculations by a two-variable method for transonic flows over an aerofoil where the wall pressure gradients were mild (i.e. the supercritical region was contained within the working section). These calculations (Ashill and Weeks [6], Rueger et al [26]) indicate that, when use is made of wall-pressure measurements in a two-variable method, the boundary-layer effect is not significant. The reason for this is that the wall pressures contain some information on the effect of the wall boundary layer on the flowfield. However, more recent work by Ashill et al [5] suggests that the effect needs to be allowed for with wall-pressure methods as Mach number approaches unity when the pressure gradients at the wall induce larger changes in boundary-layer thickness than at lower speeds. Similarly, the effect may well need to be represented for flows over high lift wings at low speeds where the pressure gradients induced at the walls can be relatively large.

In summary, for models at cruise conditions, the effect on calculated wall-induced velocities of the interaction between the inviscid flowfield and the wall boundary layers is likely to be insignificant except at high subsonic speeds, provided that a method based on wall-pressure measurement is used. More generally, the effect is likely to be important when the wall boundary layer is close to separation and may therefore be important for high-lift models at low speeds. Care should therefore be taken to monitor wall

[1] This approach would need to be modified for the lifting case where significant variations in boundary-layer thickness would be expected around the working section.

pressure distributions so that, if in doubt, calculations can be made of wall boundary layer development relative to empty-tunnel conditions.

4.2.3 NUMERICAL APPROXIMATIONS

Provided that the effect of the wall boundary layers can be ignored the effect of the walls may either be represented by the classical method of images (as in the wall pressure signature method) or by a distribution over the walls of elementary source doublets or horseshoe vortices (as in the two-variable method). In the former case consideration needs to be given to the numerical convergence of the doubly-infinite series and methods of accelerating convergence may need to be considered. One such, which has been applied by Isaacs [19] to the case of sources within wind tunnels of rectangular cross section, involves replacing the source images far from the walls by a source sheet. Analytical relationships may be used to replace double summations by rapidly convergent single series (Glauert [12], Garner et al [11]).

A method of representing the elementary source doublets by constant-density panels in the two-variable method is described in Section 4.3. An approximation to the alternative horseshoe-vortex approach is described by Ashill and Weeks [6]. So long as wall interference is not required close to the wind-tunnel walls a simple numerical integration procedure may be used to evaluate the integrals (e.g. Simpson's rule). However, if this is not the case special treatment of the singular integrals will be required. This may be done by using a panel method analogous to that described in Section 4.3.

4.2.4 CHOICE OF METHOD

Faced with the choice of the two wall-pressure methods, the wind-tunnel engineer needs to know their relative advantages or disadvantages. For attached flows typical of transport aircraft models at cruise conditions the wall-signature method is easy to apply and requires only a small number of wall-pressure measurements (Isaacs [19]). The model may be represented without difficulty by distributed singularities. The two-variable method, on the other hand, needs no model representation, as noted before, but requires many wall pressure measurements, typically of the order of 100 (Ashill and Weeks [6]). For this reason, a wall-signature method has been favoured for correcting data for blockage in tests on conventional aircraft models at high subsonic-speed cruise conditions in the 8ft x 8ft Tunnel at DRA Bedford.

For flows over aircraft models at high lift, the problem of model representation is more difficult and requires some experience in determining suitable distributions (see Section 4.2.6 and Section 8). However, as for high-speed testing, only a small number of wall-pressure measurements is needed. This contrasts with the two-variable method, which, as at high speed, needs a large number of wall-pressure measurements (Ashill and Keating [4]). On the other hand, for complex flows, such as those as studied by Ashill and Keating over a combat-aircraft model at high lift, the ability to obtain wall-interference without the need to know anything about the flow over the model is a clear advantage of the two-variable approach.

Wall boundary condition methods need only be used where classical methods, based on linear theory, cannot be applied or are expected to fail. However, where possible, calculations should be performed by a classical image method, if only as a check that the results obtained from a wall boundary condition method are sensible. As a general rule, it is recommended that wall-induced velocities should be calculated by more than one method.

4.2.5 MEASUREMENTS AND ANALYSIS OF WALL PRESSURES

4.2.5.1 WALL PRESSURE-SIGNATURE METHODS

It is self evident that success in using the wall pressure signature approach rests in measuring the signatures properly. The signal level can be small for small or low-drag models and imperfections in the tunnel, its instrumentation and its operation can easily compromise the pressure-signature measurements.

An ideal pressure signature requires:

a) A test section length of 2.5 to 3.0 hydraulic diameters. This is rarely achieved in existing general purpose tunnels. The pressure signature peak, which typically lies aft of the model, should be between 35% and 40% of the test section length from the start of the test section.

b) Smooth data with local inconsistencies and errors due to orifice and test section surface characteristics removed. This involves referencing all signatures to the appropriate 'empty-tunnel' condition, which might include model supports (sting, mounting struts, etc., as discussed in section 1.2, see also section 8.3.2).

c) High quality pressure instrumentation and proper transducer ranging.

d) Well-defined asymptotes at the upstream and downstream ends of the signature. The front of the signature should asymptote to the test section reference pressure. An offset asymptote can be handled successfully provided that it is well defined.

Figure 4.10 shows three pressure orifice distributions used in the Lockheed wind tunnels and a suggested distribution that will be discussed below. All four examples involve tunnels with B/H = $\sqrt{2}$. The orifice X-locations are normalised on working-section width, B, and a sub-scale based on hydraulic

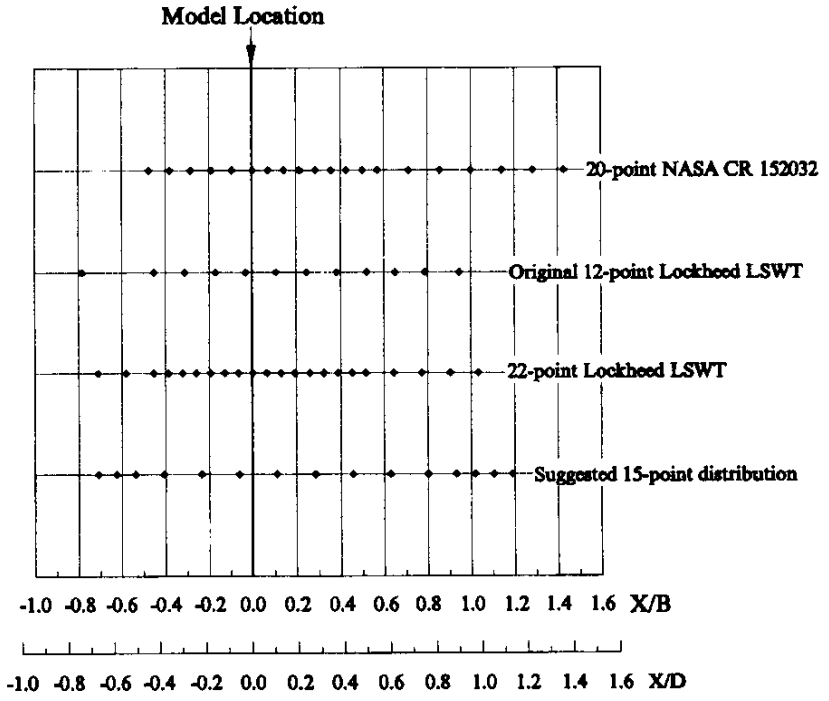

Figure 4.10 Typical orifice locations for the pressure signature method

diameter, D, is provided. Four-wall application is preferred but practical considerations may preclude floor-mounted orifices, particularly in large tunnels. This is discussed further in Section 8.3.2. The first distribution (the upper set) was employed in the (previously) Lockheed 30" x 43" MTF Wind Tunnel during the development of the wall pressure signature method for powered models (see for example Hackett and Boles [15]. To provide sufficient length for large wakes to develop, the test section length was doubled, leaving the model in its original position. This placed the model at approximately a quarter of the test section length from the entry point. The second example shows the system originally installed in the Lockheed 231/4 ft x 161/4 ft Low Speed Wind Tunnel. There are too few orifices and the signature is too short for general purpose testing but, with care, the system can be used for car testing. The greatest difficulty with this particular arrangement lies in obtaining sufficiently accurate wake source values and there is likely to be an adverse impact on calculations of the wake-induced drag increment (see Section 6.2.6 and 8.3.1.5). The third example shows a preferred arrangement for this tunnel. The last example is a further orifice arrangement suggested for test sections of insufficient length. Point concentration has been increased towards the end of the signature in an attempt to capture the asymptotes more successfully. The added points should be used as part of a larger array when fitting the asymptotes.

When setting up a tunnel system to measure pressure signatures, the following additional sources of trouble should be borne in mind:

i) bad readings from failed or failing pressure transducers.

ii) influence of the model and its images beyond the walls on the reading of the tunnel reference pressure. This problem can sometimes be corrected by regarding the reference pressure reading as part of the wall pressure signature.

iii) interference from model-induced distortions (relative to empty test section conditions) of the wall boundary layers. In extreme cases, where a high energy jet hits a tunnel wall, for example, flow control may be needed at that wall (see Section 8.3.1).

iv) insufficient sensitivity and/or accuracy of the pressure instrumentation.

v) an insufficient number or poorly selected distribution of pressure orifices.

Human monitoring of each pressure signature is an unrealistic and costly burden, and computer monitoring has not been used, as far as is known, because of the difficulty of doing so. This is a fertile area for the use of intelligent systems.

4.2.5.2 TWO VARIABLE METHODS

Most of the points made above in connection with the measurement of wall pressure signatures apply to two variable methods. However, there are considerations special to two variable methods which need to be borne in mind, as discussed below.

As noted before the streamwise velocity required as a boundary condition is usually determined from wall pressure measurements using the linear form of Bernoulli's equation. This may be justified if the perturbations in streamwise velocity at the walls are small compared with free-stream speed. If these perturbations are not 'small', it may be necessary to solve Euler's equation for the flow at the measurement surface given the pressure distribution (Ashill and Keating [3] and Maarsingh et al [23]). The use of a non-linear relationship to determine streamwise velocity can only be justified at low speeds when the governing equation for the inviscid flow, Laplace's equation, is 'exact'. At high subsonic speeds, where the linearised potential equation is solved, no increase in accuracy can be expected from refining the

estimate of wall streamwise velocity.

For the application of the two variable method it is recommended that the choice of wall orifice locations should be determined and perhaps optimised[2] by prior calculation using 'exact' solutions from classical linear theory. In these calculations an effort should be made to simulate as closely as possible the flow around the models, bearing in mind the different types of flows likely to be studied. Such a procedure was described by Ashill and Weeks [6] for a wind tunnel of square cross section and later applied to a low-speed wind tunnel of rectangular (b = 4m x h = 2.7m) cross section by Ashill and Keating [4].

Results of such assessments are shown as test cases in Figures 4.11, 4.12 and 4.13 for a floor mounted half model in the rectangular working section noted above. In the first test case the model wake is represented by a point source (Figure 4.11): in the second test case model volume is simulated by a source and sink (Figure 4.12) while, in the third test case, the lift is simulated by a horseshoe vortex (Figure 4.13). Linear theory is used to supply values of streamwise velocity at the positions of the wall orifices and this information is then used in calculations of wall-induced velocities at and along the model axis by the two-variable method. These comparisons confirmed the suitability of the choice of orifice number which, as noted in Section 4.2.1, was about 100, the orifices being placed about one tunnel breadth upstream and downstream of the model centre-line. However, these studies and others described by Rueger et al [28] suggest that the two-variable method is 'robust' in that pressure orifices can be removed without significantly affecting the accuracy of the method. Sensitivity studies such as these should be performed before any test and should form the basis for the assessment of the requirements for new wind tunnels. For existing wind tunnels, any shortfall in the number of wall holes can be made good with static tubes or static rails attached to the tunnel walls.

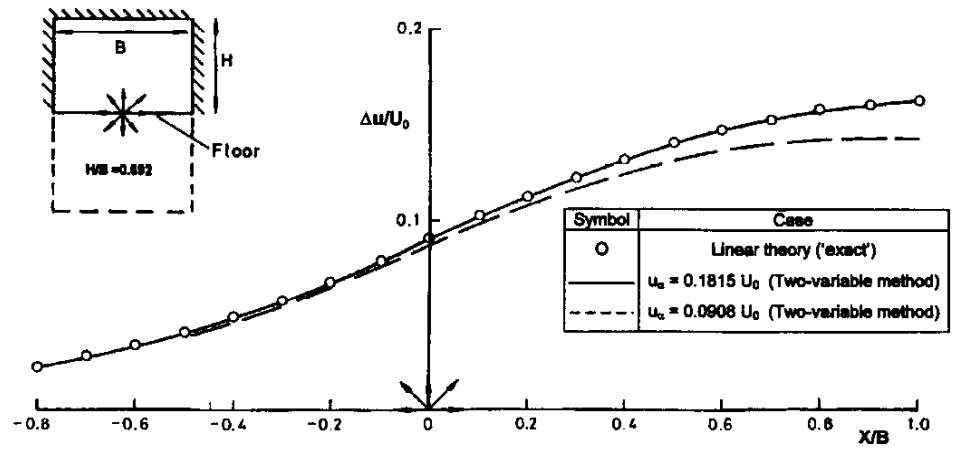

Figure 4.11 Test case 1. Point source. Blockage at 'floor' line

[2] Here 'optimised' is used in the sense of meaning minimising the number of orifices for a certain level of accuracy.

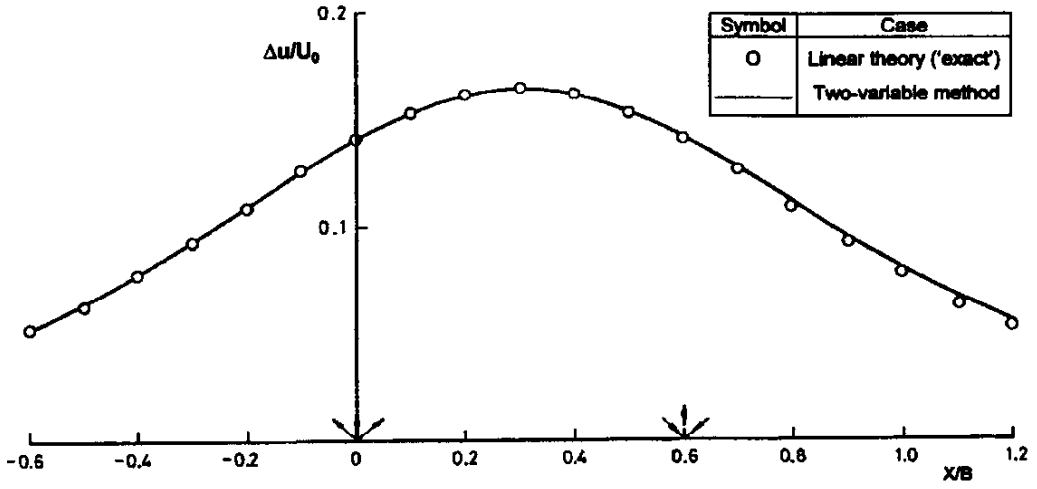

Figure 4.12 : Test case 2. Point source and sink. Blockage increment of velocity at 'floor' centre line

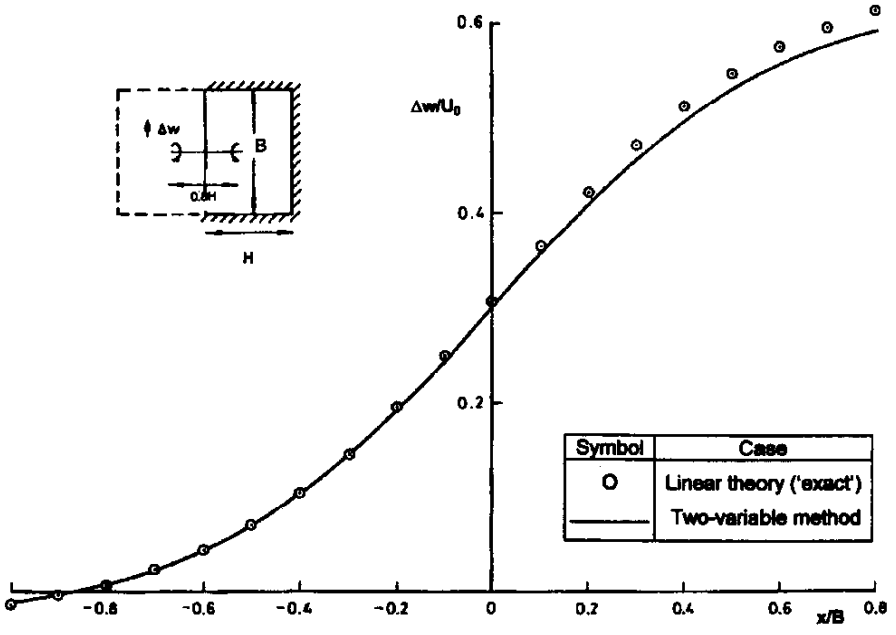

Figure 4.13 Test case 3. Horseshoe vortex. Wall-induced upwash at centre-span of vortex

An alternative approach, used by Ashill and Weeks [6], Ashill and Keating [4] and more recently by Rueger et al [28], assumes the working section to be of infinite length. The effects on the induced velocities in the region of the model of the singularities on the upstream and downstream faces are then ignored. The upstream value of the pressure increment is taken to be zero while the downstream value can be determined from momentum considerations (Ashill and Keating [4]). The blockage in the region of the model ($0<x/B<0.6$) is not sensitive to errors in the far-downstream value of the increment in pressure coefficient or velocity increment, u_∞, as may be inferred from Figure 4.11. Here an error of as high as 50% in this value causes errors of only about 5% in the blockage increment in the vicinity of the model. The pressure increments between either the most upstream or most downstream orifices and the limiting

values are obtained by interpolation assuming an exponential variation as expected from classical linear theory of wall interference for solid-wall wind tunnels. Calculations using classical linear theory (Ashill and Keating [3]) suggested that the length upstream and downstream of the model where wall pressures are measured should be approximately one working section breadth. Again, however, the suitability of the choice should be checked for individual cases.

The measurements of wall pressures should be referred to empty-tunnel conditions[3]. This needs to be done to allow for:

a) the likely non-cylindrical nature of the tunnel walls and the growth of the wall boundary layers in the empty tunnel;

b) imperfections in the wall holes; and

c) static-pressure errors due to hole size (Shaw [29] and Franklin and Wallace [9]).

Wind-tunnel users should not be surprised to find that, before being referred to empty-tunnel conditions, wall pressure distributions contain a significant degree of scatter, due mainly to effect b). However, when 'tared' to empty-tunnel conditions, smooth distributions may be expected. Where a two-variable method is used, the pressures should be checked for any faulty readings and removed prior to interpolation of the pressure data.

Consideration needs to be given to the interaction between the model supports and the tunnel walls. In some cases, the supports may intersect the tunnel walls. This poses problems because of the need then to measure a large number of pressures in the region of the supports where pressure changes rapidly. One possible way of avoiding this difficulty is to define the 'empty tunnel' as the wind tunnel including the supports but excluding the model, as previously suggested in Section 1.2. This glosses over the problem of allowing for any interaction between the model and support flowfields which has to be considered separately.

Ideally, the reference pressure should be measured sufficiently far upstream not to be affected by the presence of the model. Fortunately, for solid-wall tunnels, the combined direct and wall interference effect decays exponentially with distance, as implied before, so that the effect on the reference static pressure is likely to be negligible, at least for a wind tunnel with a working section of reasonable length. If, for any reason, the reference wall hole is affected by the presence of the model, it may be possible to invoke the auto-corrective character of the two-variable method (Mokry [25], see also Section 4.3). What this means is that the method substantially corrects for any error in reference pressure, a small residual error remaining owing to extrapolation to a 'false' zero far upstream.

Owing to the fact that the two variable method involves integration's, wall-induced velocities determined by this method tend to be insensitive to random errors in wall pressures. Nevertheless, wall-pressure distributions should be carefully monitored to ensure that the calculations of wall-induced velocities are not corrupted by erroneous pressure measurements. As mentioned in Section 4.2.5.1, this suggests the need for intelligent systems to remove such data before the calculations are performed.

Systematic errors will arise from inaccuracies in transducer calibrations, but these can be estimated by applying the errors as small perturbations to the pressure or streamwise velocity distributions in the method. Such studies are an important prerequisite for establishing the errors in the method.

---

[3] Empty-tunnel wall-pressure data will normally be taken during the calibration of the wind tunnel. Details of the calibration procedure for testing at high subsonic speeds in a solid-wall tunnel are given by Isaacs [19]. He demonstrated the importance of allowing for the direct and blockage effects of the calibration probe when determining 'empty-tunnel' static pressures at high subsonic speeds.

4.2.6 Model and Tunnel Representation when Using the „Matrix" Version of the Wall Pressure Signature Method.

4.2.6.1 Introduction

Section 4.2.5.1 gave general guidance on the installation and use of wall pressure orifices and their application to pressure-based wind tunnel correction methods. The recommended geometries were based largely on ad hoc experience, extending in some cases over a decade or more. However there was no reference to the relationship of the orifice configuration to the model under test and no indication of how an orifice system might be optimised for a given model. The present section will address these and other practical issues in a systematic way, including reviews of which walls should be instrumented, length of orifice rows and orifice spacing.

4.2.6.2 Basic Approach

The 'matrix' version of the pressure signature method employs vortex, source and doublet singularities on the model at fixed locations that correspond to matrix columns (see Hackett et al [18]). Sensing locations on the tunnel walls (pressure orifices) correspond to the matrix rows. The form of the equation is shown below:

Influence Coefficients for U-component at walls	•	Singularity strengths	=	Measured or reference U-components at walls

The matrix elements are the U-component interference coefficients for the model singularities, with their tunnel images, at the orifice locations on the tunnel surfaces (see Equation 4.11 and the subsequent discussion). In practice it is found that matrix conditioning is poor and solution oscillations that propagate into the interference field are not unusual. Since matrix conditioning depends on the particulars of both rows and columns, it is difficult to make recommendations concerning orifice spacing, for example, without reference to what the model is and how it is represented. Model representation and orifice geometry will therefore be addressed using an example derived from an actual test. The approach that will be described below may be applied to other geometry's, as needed.

The example cases will be limited to axial velocity interference, which is found to be more challenging than upwash interference in problems of the present type. Experience shows that, when the axial flow interference is calculated correctly, the upwash interference is reliable.

4.2.6.3 Model Geometry and its Representation

The test example involves a flat plate model that represents the plan view of a modern fighter aircraft. Such a model was tested and wall pressure data and analyses are available, though they will not be employed directly here. Figure 4.14 shows the model and tunnel details. The model was mounted with its trailing edge 0.99 ft above the tunnel centre plane and its nose 3.45 ft below the tunnel roof. The cross-effects between lift and blockage were therefore very significant. The program is fully three dimensional and off-centre effects are included in all analyses. The model angle-of-attack was near stall and the measured wind-axis C_L and C_D were 1.17 and 0.91 respectively.

Figure 4.14 includes a sketch of the model with line singularities at seven locations along the chord. A horseshoe vortex, a line source, and a forward-directed line doublet were placed at each location, giving a total of twenty-one elements for the case shown. Line doublets, which were not used in previous solutions of this type, have been included to improve the representation of flow closure.

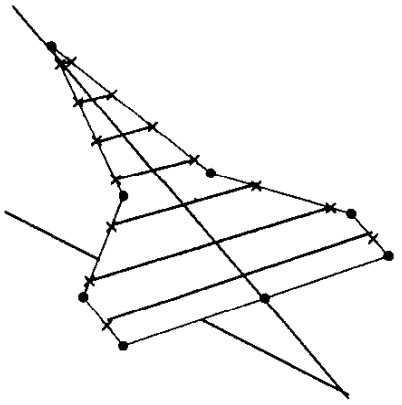

TUNNEL :
B = 23.25 ft, H = 16.25 ft
Orifices from -18 to + 20 ft, 2 ft spacing
Model TE 0.99 ft above tunnel centerline
Model nose 3.45 ft below tunnel roof

MODEL :
Double-delta planform
Span = 5.56 ft, Length = 6.38 ft
α = 35.34 DEG C_L = 1.17, C_D = 0.913
Ref Area = 15.63 sq ft, S/C = 0.0414
7 Horseshoe vortices
7 Line sources
7 x-directed Line doublets

Figure 4.14 Model and tunnel details for baseline case

4.2.6.4 REFERENCE CASE

To provide a well-controlled example, a reference case was generated using a theoretical, uniformly loaded model with the C_L and C_D values quoted above. The lift and drag loads were distributed uniformly, using the seven vortex and seven source elements shown in Figure 4.14. Line doublet strength was selected by subtracting the calculated vortex-plus-source signature from measured data and matching the residue.

For the studies below, a reference wall signature was calculated using the reference singularity strengths just described. This becomes the column vector on the right-hand side. A corresponding reference interference curve was calculated at positions along the model centreline. As a first check, the solution singularity values are compared with the reference values. Exact agreement is desirable but not essential for good interference solutions. However, excessive oscillations in singularity strength lead to incorrect interference. The obvious second check is to ensure that interference distribution calculated using the returned singularities agrees with the reference interference curve.

4.2.6.5 THE SOLVER

A solver is used that employs a proprietary orthonormalisation scheme. Its major advantage is that it detects near linear dependence between columns and rejects the appropriate column. This process is controlled by a user-defined variable 'TOLC' (TOLerance for Columns). A zero value of TOLC leaves the original matrix intact. Least-squares solutions are obtained when the row and column counts differ.

4.2.6.6 WALL ORIFICE CONFIGURATIONS

The left-hand side of Figure 4.15 defines orifice configurations evaluated in the present study. Case 1, the baseline, has orifices on the centrelines of the roof, floor and left wall of the tunnel. The right wall data is redundant for the present unyawed cases. For Case 1, some twenty orifices per wall extend from about one tunnel diameter ahead of the model to one diameter behind it. Cases 2 and 3 explore the effects of shortening all signatures. Cases 4 and 5 investigate the effects of doubling the orifice spacing, while

Case no.	Orifice Configuration	Matrix R x C		Sig RMS Error		Interfer. RMS Error	
		BASIC R x C	OPT R x C	BASIC x 10^3	OPT x 10^3	BASIC x 10^3	OPT x 10^3
1	Baseline: roof, left wall & floor, X = - 18.0 to + 20.0 ft by 2.0 ft	60 x 21	60 x 14	0.368	0.015	0.0082	0.0466
2	X = - 10.0 to + 10.0	33 x 21	33 x 14	2.792	0.012	4.7418	0.0497
3	X = - 4.0 to + 4.0	15 x 21	15 x 10	0.719	0.015	13.8500	0.0147
4	Baseline with odd points only	30 x 21	30 x 11	0.122	0.019	0.2773	0.0542
5	Baseline with even points only	30 x 21	30 x 12	2.134	0.015	4.6750	0.0465
6	All four walls	78 x 21	78 x 14	1.291	0.014	1.5135	0.0486
7	**Roof and left wall**	40 x 21	40 x 13	0.125	0.009	0.0960	0.0512
8	Roof only (C>R)	20 x 21	20 x 10	0.018	0.004	1.0690	0.1537

Fig 4.15 Effect of column optimisation for 7+7+7 initial elements and various wall orifice configurations.

retaining the baseline total length. The effect of adding back the right-hand wall is explored in Case 6. Cases 7 and 8 investigate roof-and-left wall and roof-only cases.

4.2.6.7 CASES WITH NO ELEMENT OPTIMISATION (TOLC = 0)

The "7 + 7 + 7" case reproduces the reference solution only for the baseline orifice configuration. Earlier studies, employing a similar "5 + 5 + 5" element arrangement closely followed the original input for all cases except the very short signature, Case 3. The singularity strengths in the 5 + 5 + 5 Case 3 oscillated strongly and the interference results were useless. This is probably attributable to the shortness of the signatures.

Repeating the same exercise for the 7+7+7 geometry gave noticeable RMS errors for the signature fit (Figure 4.15, column 5) and mainly oscillating singularity solutions. Case 1, the baseline, gave good interference results (Figure 4.16, upper plot) and Case 7 (roof and left wall) was probably acceptable. Of the remaining solutions, only Case 4 (doubled orifice spacing, "odd" points) was "on the page." However Case 5 ("even" points) displayed matrix instability and, like the remaining orifice configurations, gave interference values that were several times too high. Many of these curves oscillated and were obviously wrong, but those that were smooth could have been misleading had the reference curve not been available.

4.2.6.8 CASES WITH ELEMENT OPTI MISATION

On increasing the control parameter, TOLC, the column count for the baseline wall orifice configuration decreased monotonically from 21 to 12 over the range considered. The amount of column reduction depends upon the orifice configuration. As TOLC was increased, two minima occurred in the RMS error of

the fitted wall signature: experience has shown that the second gives superior results. The right half of Figure 4.15 summarises the RMS errors in the wall signature and interference curve fits. The column count at the optimum varies between ten and fourteen elements depending upon the orifice configuration. The optimised results show a very significant improvement in the signature fitting errors compared with the basic solution with the full 7 + 7 + 7 element count.

The lower plot of Figure 4.16 shows U-component interference curves at the model centreline for the optimised cases. The corresponding RMS errors are given in Figure 4.15. Most of the interference solutions are bunched at a level approximately 0.0002 higher than the reference curve. This represents acceptable accuracy and the fact that the curves are tightly grouped is probably the more important. Case 8, with only roof orifices, gave the only unsatisfactory solution. Case 3 was in close agreement with the reference curve but this is considered coincidental.

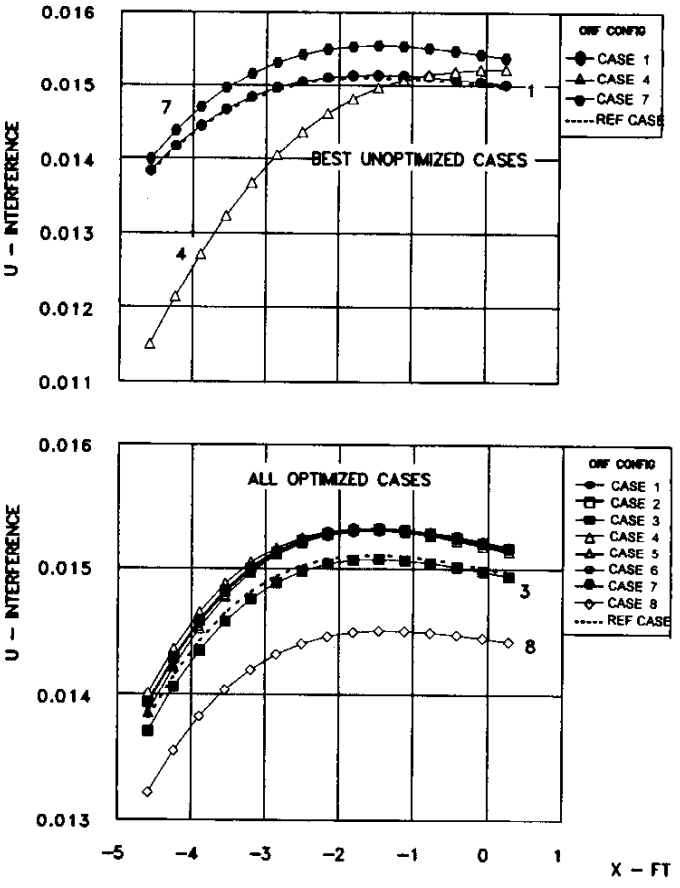

Figure 4.16 Interference for unoptimised and optimised cases (7 + 7 + 7 initial elements)

The fact that the unoptimised Case 8 gave a low RMS error for the signature fit yet a high interference RMS error requires comment. If the influence matrix is square and is solved successfully, the signature fit RMS error will be near-zero (by definition) whether or not the reference singularity values are returned. If fact, the singularity strengths may oscillate and produce an unacceptable interference result. This is what happened for the unoptimised Case 8, for which the influence matrix is nearly square. Obtaining a good signature fit does not guarantee good interference values, particularly if the matrix is near-square.

Figure 4.17 identifies the singularities retained for the various 7 + 7 + 7 solutions. Most of the vortex elements were usually retained and most of the doublet elements were usually rejected. The sources and doublets just ahead of the trailing edge were always retained, as were the sources near the apex of the delta. The consistent pattern of singularity locations in Figure 4.17 suggests that such a pattern might be used successfully without an optimiser for this configuration and angle of attack.

Increasing the column count first to 10 + 10 + 10 and then to 15 + 15 + 15 was beneficial. The eight cases were increasingly tightly grouped and the groups lay increasingly close to the reference curve. Evidently, with a larger choice of element locations afforded by the larger element counts, the optimiser can choose a better element arrangement.

Wall config		1	2	3	4	5	6	7	8
Vortex elements	1	*	*	*	*	*	*	*	*
	2	*	*	*	*	*	*	*	*
	3	*	*	*	*	*	*	*	*
	4	*	*	*	*		*	*	*
	5	*	*			*	*	*	*
	6	*	*	*	*	*	*	*	*
	7	*	*	*	*	*	*	*	
Source elements	8	*	*	*	*	*	*	*	*
	9	*	*			*	*	*	*
	10				*				
	11	*	*			*	*	*	
	12	*	*				*		
	13								
	14	*	*	*	*	*	*	*	*
Doublet elements	15								
	16								
	17								
	18								
	19			*	*				
	20	*	*			*	*	*	
	21	*	*	*	*	*	*	*	*
TOTAL	**21**	**14**	**14**	**10**	**11**	**12**	**14**	**13**	**10**

* Filled squares denote retained matrix columns

Fig 4.17 Element disposition for optimised cases

4.2.6.9 REVIEW

It was shown above that there are two practical approaches to configuring the model elements. If "straight" solutions are to be used, with no column optimisation, then the element count must be kept low (5 + 5 + 5 in the case above) and the singularity solutions must be watched carefully for undue oscillation. In cases of doubt, the element count should be reduced. If an optimisation scheme is used the number of elements can be increased significantly (to 15 + 15 +15, say). An increase is not essential when using an optimiser but, as was shown above, a better fit to the reference solution is obtained. Whichever strategy is adopted, it is important to ensure that the elements are placed appropriately to capture the model's loads. It is also beneficial to employ "over square" matrices with significantly more rows (orifices) than columns (model elements). This makes the RMS errors in fitting the wall signatures more meaningful.

The baseline case, above, is a good orifice arrangement for the model configuration employed here. Having a lift coefficient that is close to the maximum , it is one of the most important low speed cases and may also be among the most demanding. The first optimum for the 7 + 7 + 7 configuration (not shown) was helpful in identifying marginal wall configurations. Cases 2 and 3 showed that it is inadvisable to shorten the signatures below the Case 1 value. Cases 4 and 5 showed that orifice spacing should not be reduced. Omission of the orifices on the floor centreline (Case 7) gave surprisingly good results, which is helpful because of the vulnerability of instrumentation placed there, particularly in a large tunnel. The fact that Case 8, with roof-only data, was the weakest (Figure 4.16) comes as no surprise, since the program is being asked to distinguish between lift and blockage effects using a single signature.

4.2.6.10 Other Model Configurations

Various pressure orifice geometry's have been reviewed for an unyawed model at a single angle-of-attack and one height in the tunnel. The present study does not address the needs of other data points or other configurations. However, the baseline orifice configuration selected above is generally similar to a layout that has been used successfully in the Lockheed Low Speed Wind Tunnel for many years. In that tunnel, the wall orifices are above the centreline, to avoid windows, there are extra orifices opposite the model, and there are no floor orifices.

Despite the above, there will be occasions when more assurance is required. In such cases, a study similar to the one described in the main body of this section should be carried out. This would involve a simple theoretical model, placed at the appropriate position and attitude in the tunnel and carrying the correct loads. Wall signatures and reference interference curves should be calculated, as described above, and trial runs performed to find the best orifice and model element configurations. In facilities with an existing orifice system, its suitability can be assessed in a similar way and any additional orifices that are needed can be identified.

4.2.6.11 Three-way Interactions

Tunnel Interference is usually thought of in terms of the classical vortex, source and doublet theoretical representation of the model and its tunnel image system. Not a lot of attention has been paid, until recently, to the possibility that the model support system may also become involved in the interference process. Two examples of this surfaced during the tests upon which the above example is based. Both involved the sting support system and both represent ongoing work. The comments below should therefore be considered provisional.

In the first example, a study of model absent (sting present) and model-present pressure signatures suggested that the sting immediately aft of the model was experiencing model-induced download. Extra model elements were therefore added to those shown here to represent the forward part of the sting.

The second example involves a large floor-to-roof tower that supports the base of the sting and carries a carriage that moves vertically as the sting pitches. Being in the wake of the model, it was found that the loads on the tower, too, changed with the model present. Analyses based solely on model out datum corrections were inadequate, even though the tower was present for the datum measurements and the sting pitch setting was appropriate. In fact, the tower appeared to the flow as a vertical line source whose presence destabilised the pressure signature solutions. Adding a floor-to-roof line source, of unknown strength, improved the solutions. The lesson learned was that, if the model flow interferes with tunnel components and/or the model supports and the wall signatures are affected, then it is essential to represent those components in the influence matrix.

REFERENCES TO SECTION 4.2.

[1] Acum, W. E. A., 1953, "Corrections for symmetrical and swept and tapered wings in rectangular wind tunnels", ARC R&M 2777.

[2] Adcock, J. B., and Barnwell, R. W., 1984, "Effects of boundary layers on solid walls in three-dimensional wind tunnels", AIAA Journal Vol 22, No 3.

[3] Ashill, P.R. and Keating, R.F.A., 1985, RAE unpublished report.

[4] Ashill, P.R. and Keating, R.F.A., 1988, "Calculation of tunnel wall interference from wall-pressure measurements." The Aeronautical Journal, Vol. 92, No. 911, pp. 36-53.

[5] Ashill, P. R., Taylor, C. R. And Simmons, M. J., 1995, "Blockage Interference at High Subsonic Speeds in a Solid-Wall Wind Tunnel.", Proceedings of PICAST 2 - AAC 6, Vol 1, pp 81-88, Melbourne 20 -23 March 1995.

[6] Ashill, P.R. and Weeks, D.J., 1982, "A method for determining wall-interference corrections in solid-wall tunnels from measurements of static pressure at the walls." AGARD-CP-335, pp.1.1-1.12.

[7] Berndt, S. B., 1952, „Approximate calculation of the influence of wall boundary layers on solid walls in three dimensional subsonic wind tunnels.", FFA (Sweden) Report No. 45

[8] Bouis, X., 1984, "ETW specification and its vindication." Document SC-ETW/D/27 (Revision 4).

[9] Franklin, R. E, and Wallace, J. M., 1970, "Absolute measurements of static-hole error using flush transducers." J. Fluid Mech., 42, 33.

[10] Freestone, M. M., 1995, "Upwash interference for wings in solid-liner wind tunnels using subsonic linearised-theory." ESDU Data Item 95014.

[11] Garner, H.C., Rogers, E.W.E., Acum, W.E.A. and Maskell, E.C., 1966, "Subsonic wind tunnel wall corrections.", AGARD-AG-109.

[12] Glauert, H., 1942, "The elements of aerofoil and airscrew theory", Cambridge University Press, Fourth Impression.

[13] Göthert, B., 1940 "Windkanalkorrekturen bei hohen Unterschallgeschwindigkeiten unter besonderer Berücksichtigung des geschlossenen Kreiskanals. Deutsche Luftfahrtforschung Forschungsbericht 1216 (translated as NACA Tech Memo 1300).

[14] Hackett, J.E. and Wilsden, D.J., 1975, "Determination of low speed wake-blockage corrections via tunnel-wall static pressure measurements." AGARD-CP-174, pp. 22.1-22.9.

[15] Hackett, J. E., and Boles, R. A., 1977, „Ground simulation and Wind tunnel blockage for a swept jet-flapped wing tested to very high lift coefficients." NASA CR 152,032 (also AIAA 74-641)

[16] Hackett, J.E. and Wilsden, D.J., 1979, "Estimation of tunnel blockage from wall pressure signatures: a review and data correlation." NASA CR-152241.

[17] Hackett, J.E., Wilsden, D.J., and Stevens, W.A., 1980, "A review of the wall pressure signature and other tunnel constraint correction methods for high angle-of-attack tests." AGARD-R-692.

[18] Hackett, J. E., Sampath, S., and Philips, C. G., 1981, "Determination of wind tunnel constraint effects by a unified wall pressure signature method: Part I, Applicationa to winged configurations." NASA CR 166,186.

[19] Isaacs, D., 1969, "Calibration of the RAE Bedford 8ft x 8ft wind tunnel at subsonic speeds, including a discussion of the correction to the measured pressure distribution to allow for the direct and blockage effects due to the calibration probe." ARC R&M 2777.

[20] Jones, R. T. And Cohen, D., "High speed wing theory." Princeton Aeronautical Paperbacks (No. 6), Princeton University Press, 1960.

[21] Lewis, M. C. And Goodyer, M. J., 1995, "Initial Results of an Experimental Investigation into the General Application of Transonic wind Tunnel Wall Corrections." Proceedings of PICAST2 - AAC 6, Vol 1, pp 71-79, Melbourne 20-23 March 1995.

[22] Lewis, M.C., 1988, "Aerofoil testing in a self-streamlining flexible walled wind tunnel." NASA CR-4128.

[23] Maarsingh, R.A., Labrujere, Th.E., and Smith, J., 1988, "Accuracy of various wall-correction methods for 3D subsonic wind-tunnel testing." AGARD-CP-429, pp.17.1-17.13.

[24] Mokry, M. and Ohman, L. H., 1980, „Application of the Fast Fourier Transform to two-dimensional wind tunnel wall interference." Journal of Aircraft, Vol. 17, No. 6, pp 402-408

[25] Mokry, M., 1989, "Residual interference and wind tunnel wall adaptation." USA AIAA-89-0147.

[26] Pindzola, M. and Lo, C. F., 1969, "Boundary interference at subsonic speeds in wind tunnels with ventilated walls" AEDC-TR-69-47.

[27] Pistolesi, E., 1933, Considerazioni sul problema del bi-plane, Aeronautica, Rome 13, 185

[28] Rueger, M., Crites, R. And Weirich, R., 1995, "Comparison of conventional and emerging ("measured variable") wall correction techniques for tactical aircraft in subsonic wind tunnels (invited paper) AIAA 95-0108, 1995.

[29] Shaw, R., 1960. "The influence of hole dimensions on static pressure measurements". J. Fluid Mech., 7 , 550.

[30] Steinle, F. and Stanewsky. E, 1982, "Wind tunnel flow quality and data accuracy requirements", AGARD-AR-184.

[31] Taylor, C. R., 1996, "A note on some fundamental concepts in the theory of wind-tunnel wall constraint and its application", DRA/AS/HWA/TR96055/1

[32] Thom, A., 1943, "Blockage corrections in a closed high-speed tunnel." ARC R&M 2033.

[33] Ulbrich, N., Lo C. F. and Steinle F. W., Jr., 1992, "Blockage correction in three-dimensional wind tunnel testing based on the wall signature method" AIAA 92-3925 .

[34] Ulbrich, N. and Steinle, F.W., Jr., 1994 "Real-time wall interference calculation in three-dimensional subsonic wind tunnel testing", AIAA 94-0771.

[35] Ulbrich, N. And Steinle, F. W., Jr., 1995 "Semi-span model wall interference prediction based on the wall signature method", AIAA 95-0793.

4.3 VENTILATED TEST SECTIONS

Contemporary developments in wall correction methods for ventilated wall test sections have shown an increasing reliance on measurements of wall boundary data. An excellent work recognising these new trends in two-dimensional testing has been produced by the Group for Aeronautical Research and Technology in Europe (GARTEur [26]).

Although it has been demonstrated both experimentally (Chen and Mears [12], Jacocks [33], Matyk and Kobayashi [45], and Crites and Rueger [15]) and computationally (Chan [11]) that the cross-flow properties of ventilated walls are non-linear (even strongly) and dependent on the wall boundary layer development, the correction techniques based on idealised, linear boundary conditions have retained a great deal of appeal. The main reason is that the parameters in the empirical boundary conditions (porosity or slot parameters) can usually be tuned so as to provide correlation of key aerodynamic quantities for two or more different-scale calibration models in the same facility (Firmin and Cook [20]). An approach less sensitive to wall Reynolds number effects (Aulehla [6]), is to adjust the boundary condition parameters in such a way that the corrected data agree with those measured on the same model in a very large facility, assumed to be interference free (Binion and Lo [8], Starr [72], and Sickles and Erickson [66]). The obtained values of these parameters may then used to correct the wind tunnel data of other models which are similar to the calibration models in shape and size. Besides simplicity of application, the most appealing aspect of this (classical) approach is that it generates consistent, smooth corrections: if the measured dependence of C_L on α or C_D on C_L is smooth, so will be the corrected one. The corrections are predictive, which means that if we can estimate what the measured forces will be, we will also be in position to predict the corrections, in advance of a wind tunnel test, see Chapter 3.

A practical advantage of the classical methods is also that there is no need to measure quantities other than those directly related to the test model. However, if the static pressures at the test section walls happen to be measured and compared with those predicted using the idealised boundary conditions, substantial differences are likely to be uncovered. One of the possibilities to reduce this inconsistency in wall interference evaluation is to locally modify the wall boundary conditions in such a way that they provide the best possible agreement with the measured wall data (Mokry et al. [47], Jones, D.J. [34], Vaucheret [77], and Piat [58]. The values of the parameters in the boundary conditions will of course differ from test to test. Using this approach, the modified boundary conditions, regardless of their possible physical significance, provide no more than a fit of the measured boundary data. From here on it is only a small step to realise (Capelier et al. [10]) that the measured boundary data can directly be used as input. One is not limited to measuring data from the boundary. Pressure measurements on the model can be used similarly in conjunction with calibration of selected pressures for Mach and angle of attack effects and then employing closed wall and open wall settings. The closed wall settings in conjunction with a suitable means of estimating displacement thickness and any wall divergence effects then represent a boundary condition that is sufficiently known. Corrections to the closed wall case then form a reference to the open wall case. Variation of parameters in the boundary condition for the open wall case will permit finding the parameters that produce corrections which will best satisfy the corrected closed wall results in say, a least squares sense. These results can then be compared with those determined from matching measured wall data, or vice-versa for improved confidence.

In spite of the fact that much of the empiricism of the classical correction methods is eliminated by the boundary measurement methods, it is the latter ones that are under steady scrutiny. Their general acceptance is hindered by the fact that making the required flow measurement in ventilated test sections can be a very complex task and evaluation of corrections from a larger boundary input requires a small-

scale numerical code rather than a simple formula or chart. In addition, the corrections can only be used in the "post-test assessment" mode. It is no longer possible to predict the corrections by specifying the aerodynamic forces: a wind tunnel experiment with actual wall pressure measurements needs to be performed first; and only then the corrections can be evaluated. Also, a larger experimental data input produces corrections which are "scattery" in comparison with the classical ones (Labrujère et al. [40]). This is not to say that global corrections to tunnel reference conditions can't be determined in advance. Any prior post-test corrections are candidates for developing a library of corrections with a suitable empirical analysis. In many cases, global corrections are sufficient (e.g., Goldhammer and Steinle [28])

4.3.1 ONE-VARIABLE METHOD

The method proposed by Capelier et al. [10], and in a simpler form also by Blackwell [9], is the most popular technique for the post-test assessment of subsonic wall interference from boundary pressure measurements in wind tunnels with ventilated walls. It is assumed that the velocity disturbance potential near the walls is governed by the linear Prandtl-Glauert equation,

$$\beta^2 \frac{\partial^2 \phi}{\partial x^2} + \frac{\partial^2 \phi}{\partial y^2} + \frac{\partial^2 \phi}{\partial z^2} = 0 \qquad (4.3.1)$$

and that it may be split into the free air and wall interference parts,

$$\phi = \phi_F + \phi_I \,. \qquad (4.3.2)$$

The only difference from the classical wall interference approach is in replacing the idealised wall boundary condition by the "measured" one, namely by

$$\frac{\partial \phi}{\partial x} = u \qquad (4.3.3)$$

where

$$u = \frac{U - U_\infty}{U_\infty}$$

is the measured streamwise component of perturbation velocity.

Unlike flow near the model, where stagnation and locally supersonic regions may exist, flow near the walls is significantly less perturbed so that linearisation may apply up to quite high subsonic Mach numbers. If the model is small relative to the test section and sufficiently remote from the walls, it is only when free stream Mach number is close to unity that portions of the walls become near critical or supercritical, making the assumptions of Eqs.(4.3.1)-(4.3.2) invalid.

The way Eq.(4.3.2) is usually interpreted is that ϕ_F is a disturbance velocity potential that would be generated by the model if loaded by the same aerodynamic forces in free air, and ϕ_I is the wall interference potential induced by the walls. In other words, ϕ_I is an increment to ϕ_F that makes the total satisfy the (measured) wall boundary conditions.

Provided that ϕ_F satisfies Eq.(4.3.1) near the walls, it can be represented there (and in the infinite exterior region) by internal singularities. In contrast, ϕ_I can be represented by external singularities (images). An equally justifiable assumption is that ϕ_I be non-singular, but discontinuous across the

interface between the interior and exterior flow. This latter approach is used when evaluating ϕ_I by a panel method. Regardless of the representation of the exterior fictitious flow, the key premise of subsonic wall interference theory is that ϕ_I is non-singular in the interior (including the volume occupied by the model), allowing to evaluate the velocity corrections to (uniform) wind tunnel stream as the components of gradϕ_I . Although an application of this concept is almost axiomatic in both the classical and the boundary measurement methods, one should remember that it is merely an engineering approximation, even for low-speed (incompressible) flows.

The assumptions upon which the one-variable method is based are thus the following: the axial component of wall interference velocity

$$u_I = \frac{\partial \phi_I}{\partial x} \tag{4.3.4}$$

satisfies the differentiated Eq.(4.3.1), that is

$$\beta^2 \frac{\partial^2 u_I}{\partial x^2} + \frac{\partial^2 u_I}{\partial y^2} + \frac{\partial^2 u_I}{\partial z^2} = 0 \tag{4.3.5}$$

in the entire test section interior (including the volume occupied by the model).
Using Eq.(4.3.2), the boundary values of u_I are evaluated on the measurement surface as

$$u_I = u - u_F \tag{4.3.6}$$

Here u_F is the axial component of disturbance velocity that would be induced at the location of the measurement surface by the same model in free air, at the same stream velocity, U_∞, and the same aerodynamic forces. Provided that the measurement surface is sufficiently remote from the model, we only need to know the far-field approximation of u_F .

Equations (4.3.5) and (4.3.6) specify an interior Dirichlet problem and there are a large number of methods available to solve it analytically or numerically. For simpler geometry's, closed-form solutions are obtainable using integral transforms (Capelier et al. [10]) or the Fourier method (Mokry and Ohman [49], Mokry [50], and Rizk and Smithmeyer [61]). A detailed description and coding of two of these techniques in Fortran are given by Gopinath [29].

The Dirichlet problem for Laplace's equation, to which Eq.(4.3.5) is reducible (by a co-ordinate transformation) is known to have a unique solution inside a region, provided that the boundary values are specified everywhere on its bounding surface. This guarantees that there is only one solution to u_I for the given prescribed values of u_I on the boundary. As we shall see below, the same cannot be said of the interference velocity components v_I and w_I, evaluated from the same boundary values of u_I.

A natural approach (e.g. Stakgold [71]) to solving the Dirichlet problem for Laplace's equation is to represent u_I by the double layer potential :

$$u_I = \frac{1}{4\pi} \int_S f \frac{\partial}{\partial n}\left(\frac{1}{r}\right) dS \ , \tag{4.3.7}$$

where f is the doublet density and r is the distance between the fixed observation point x_0, y_0, z_0 (where u_I is being evaluated) and point x, y, z, which runs over the surface S in the course of integration. The derivative $\partial / \partial n$ is taken in the direction of the inward normal, that is pointing into the test section interior.

If the observation point is on surface S, the integrand becomes singular, because r appearing in the denominator will be zero when the running point reaches the observation point. Nevertheless integral (4.3.7) exists; but, because of its singular nature, its value depends on which side of the integration surface the observation point lies. In other words, u_I is discontinuous across S. Taking the limit as the observation point becomes a point on the inner (flowfield) side of surface S, we obtain

$$u_I = \frac{f}{2} + \frac{1}{4\pi} \int_S f \frac{\partial}{\partial n}\left(\frac{1}{r}\right) dS \ , \qquad (4.3.8)$$

where a small circular neighbourhood of the observation point (where $r = 0$) is considered removed from the surface integration; its contribution has already been accounted for by the isolated term $f/2$.

With respect to the unknown density f, Eq.(4.3.8) can be interpreted as a Fredholm integral equation of the second kind. The solution can be obtained numerically by dividing S into panels of (piecewise) constant density f, applying Eq.(4.3.8) at panel centroids and solving the resulting system of linear algebraic equations (Mokry et al. [52]). If the walls are straight, the matrix is easily assembled using the contribution of a rectangular panel of unit doublet density, elaborated in the Appendix. The isolated term $f/2$ in Eq.(4.3.8) provides the diagonal element, or contribution of the panel to its own centroid.

The major source of inaccuracy, which is common to all wall interference methods based on boundary measurements, is incompleteness or sparseness of the experimental pressure data. The boundary values of u_I have to be interpolated or extrapolated over a complete boundary (finite or infinite), in order to make the Dirichlet problem fully defined. More specifically, the panel method will require the knowledge of u_I at all panel centroids, as shown schematically in Figure 4.18. The crosses indicate the measurement points and the solid and open circles are the panel centroids on measurement and non-measurement surfaces respectively. A variant of the panel method which does not require extensive pressure measurements or interpolation has been reported by Ulbrich and Steinle [75], [76] for full-span and half-span models with an image plate. The method employs precalculated influence coefficients for both wall panels and singularities used to represent the model at a few control points on the tunnel boundary. Known strengths of singularities from measured force and moment data and assumed distribution of loading are taken into account in determining the strength of the remaining singularities (equivalent to two unknowns) by satisfying the measured pressures in a least squares sense. The method is designed to compute global blockage and angle-of-attack corrections in near real-time. In effect, it combines the features of a direct method and a one-variable method. The application reported is for a solid wall tunnel. However, the influence method is more general and can be applied to either a porous or a slotted wall, providing that a reliable measurement of pressure at the boundary is obtained.

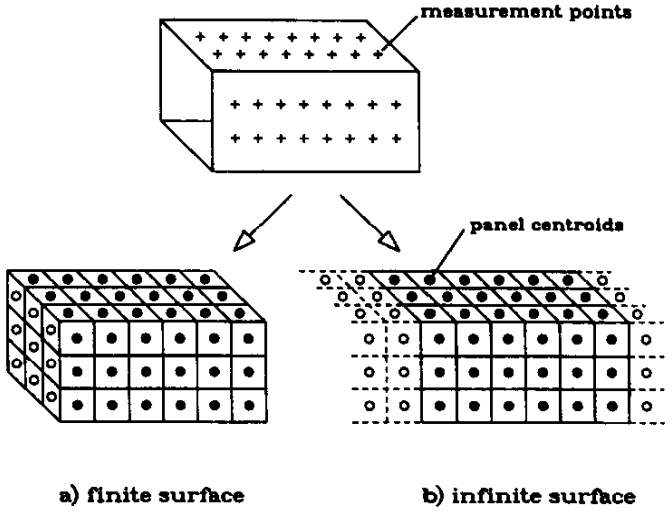

Figure 4.18 Illustrating measurement and input of boundary data

The simplest way to tell how well a proposed interpolation scheme works is to test it on a theoretical example: generate u_I by external singularities or images (Holst [32]) and check how faithfully the method reproduces u_I inside the test section from the known boundary values at the measurement points.

By nature of the solutions to elliptic equations, such as Laplace's or Prandtl-Glauert's, the evaluation of subsonic wall interference corrections from the boundary data is a smoothing operation. Unless the corrections are required to be known in the vicinity of the walls, pre-smoothing of the boundary data is unnecessary. Elimination of grossly erroneous boundary input points is an entirely different matter: although an individual disturbance will smooth out and will not likely be detectable as a localised perturbation at the model, it will influence the overall level of calculated wall interference. Another characteristic of linear subsonic wall interference, following from the so-called "max-min" property, is that the corrections at the tested model can neither be greater nor smaller than their respective maxima or minima attained at the walls

Compensation for errors of the reference velocity or pressure is another important feature of the method. An uninitiated experimenter may find it quite amazing that if we change the reference pressure on which the stream Mach number M is based slightly, then recalculate the wall C_Ps and evaluate a new ΔM, the same corrected Mach number, $M+\Delta M$, is found. Actually, the principle is nearly self-evident: if the error of the (upstream) reference velocity U_∞ is δU_∞, then the boundary perturbation velocities $U-(U_\infty+\delta U_\infty)$ will be offset by $-\delta U_\infty$ from their true value $U-U_\infty$. However, since $-\delta U_\infty$= constant is also a solution of Eq.(4.3.5), the incremental correction, being of equal magnitude but opposite sign to the reference velocity error, restores U_∞ as the true reference velocity. Naturally, the relationship between pressure and velocity requires linearisation, so that the principle is restricted to small errors (Paquet [56]). The principle may also be compromised if extrapolation of U towards the "false" upstream reference $U_\infty+\delta U_\infty$ is used (GARTEur [26]).

Similarly, in ventilated test sections the autocorrection principle establishes the correspondence between the velocity based on plenum pressure, $U_\infty+\delta U_\infty$, and the actual stream velocity U_∞. In this context each wind tunnel test with wall pressure measurements in effect is also a calibration test. Empty wind tunnel calibration, as used in the classical wall interference approach, is a poor substitute since the model influences not only the wall pressure, but also the plenum pressure (Smith [67], Aulehla [6], and Everhart and Bobbitt [18]).

A related question often asked is: if small errors of the reference Mach number don't matter is it also true that small errors of C_L and C_D don't? Unfortunately they do. Accuracy of the one-variable method is greatly dependent on accuracy with which the free air potential ϕ_F can be predicted along the boundary surfaces (GARTEur [26], Chevallier [13]). At low subsonic flow conditions, the far-field can be generated fairly well by internal singularities, determined from the model geometry and measured loading (Binion and Lo [8], Rizk and Smithmeyer [61], Vaucheret [77] and Mokry [51]). This approach becomes less reliable at high incidence cases, where the extent of separated flow regions is generally unknown. Model representation by subsonic-flow singularities needs also to be modified near critical flow conditions, see Cole and Cook [14], Kemp [37] and Al-Saadi [2]. However, when the supersonic flow regions become extensive, perhaps even reaching the wind tunnel walls, the superposition principle, on which Eq.(4.3.6) is based, will no longer apply. The linear correction method may even then go on producing numbers; nevertheless, alternative wall correction methods which respect the true, non-linear nature of transonic flow should be applied (see Chapter 5.)

In the one-variable method the transverse velocity components

$$v_I = \frac{\partial \phi_I}{\partial y} \quad \text{and}$$

$$w_I = \frac{\partial \phi_I}{\partial z} \quad (4.3.9)$$

are obtained from u_I by integrating the irrotational-flow conditions

$$\frac{\partial v_I}{\partial x} = \frac{\partial u_I}{\partial y} \quad \text{and}$$

$$\frac{\partial w_I}{\partial x} = \frac{\partial u_I}{\partial z} \quad (4.3.10)$$

The flow angle corrections are thus determined up to (unknown) integration constants. This is somewhat disappointing; however, the variations of wall induced angularity over the model can still be evaluated and a case made whether the wind tunnel test is correctable or not (Steinle and Stanewsky [73]).

In Figure 4.19 an example of corrections evaluated by the one-variable method is given for the Canadair Challenger half-model tested in the IAR Blowdown Wind Tunnel. The boundary pressures were measured by 6 static pressure tubes (2 on top, 2 on bottom and 2 on the sidewall) and the division of the test section boundary box in the x, y, z directions was $11 \times 5 \times 5$, giving a total of 215 panels. The ΔM and $\Delta \alpha$ correction contours were plotted in the horizontal plane (wing planform). There is no ambiguity in the interpretation of the ΔM correction but, as we have indicated above, the absolute level of the $\Delta \alpha$ correction is not known with certainty.

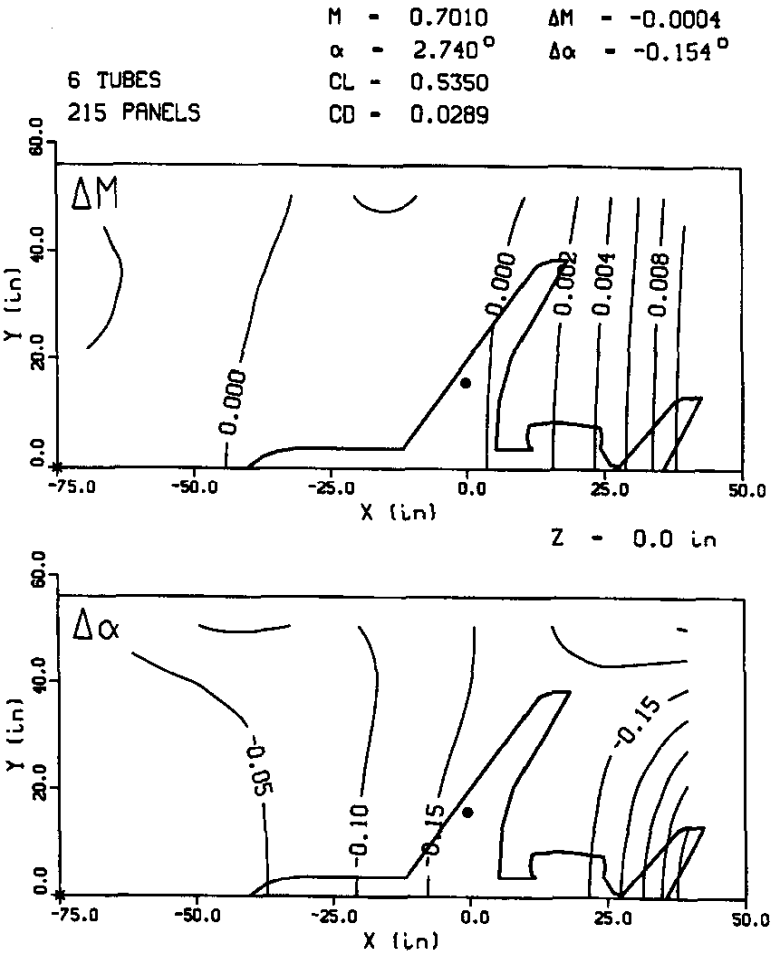

Figure 4.19 Wall corrections for a Canadair Challenger half model test in the IAR Blowdown Wind Tunnel, produced by the one-variable method

Values to the unknown angular constants can be assigned (as has been done in Figure 4.19) by assuming that flow enters the test section parallel to its axis. This is accomplished by imposing the conditions

$$v_I + v_F = 0 \quad \text{and} \quad w_I + w_F = 0 \qquad (4.3.11)$$

at an upstream axial point. If we instead imposed a condition that v_I and w_I vanish there, we would in effect assume that far upstream flow angles are the same as they would be in free air. Simple theoretical analyses contradict the latter assumption by showing that under the confinement of a constant cross-section channel the flow angles upstream of the model decay much faster with the distance from the model than they would in free air.

We can illustrate this on a simple example, which is of some relevance to testing of high-aspect ratio wings. Consider a two-dimensional vortex placed midway between two walls, as shown in Figure 4.20.

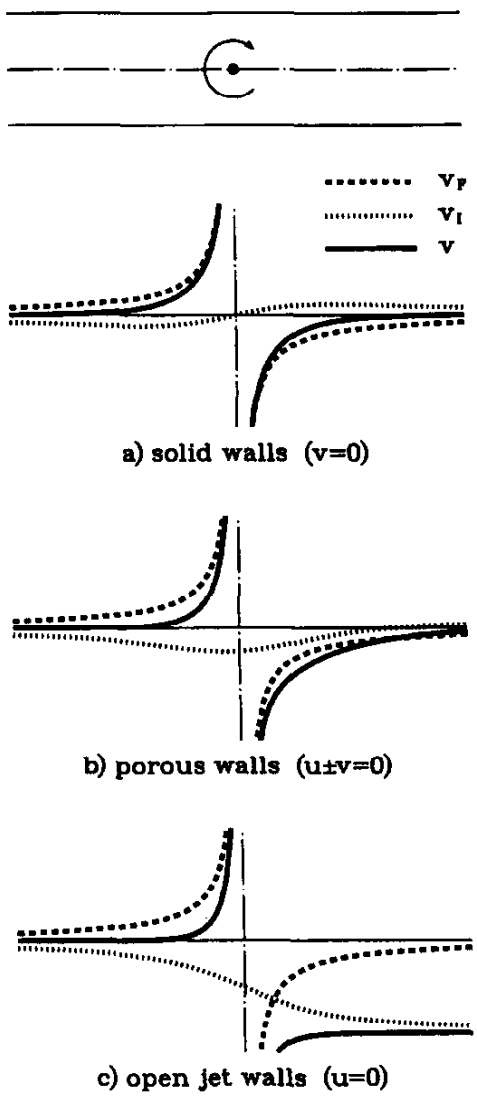

Figure 4.20 Upwash velocity along the axis of a test section induced by a point vortex

The free-air potential of the vortex is

$$\phi_F = \frac{-\gamma}{2\pi} \arctan \frac{z}{x},$$

compare Eq. (2.12). The vortex induces along the x-axis the normal velocity

$$v_F = \frac{\partial \phi_F}{\partial z} = \frac{-\gamma}{2\pi x} = \frac{-\gamma}{2h\left(\frac{\pi x}{h}\right)}.$$

The normal velocity along the axis of a closed-wall wind tunnel, as obtained by the method of images (Theodorsen, 1931), is

$$v = v_F + v_I = \frac{-\gamma}{2h \sinh\left(\frac{\pi x}{h}\right)}.$$

Evidently, the test section height h plays a key role here: if $h \to \infty$, then $v \to v_F$. However, if h is finite, then according to the l'Hospital rule

$$\lim_{x \to -\infty} \frac{v}{v_F} = 0,$$

which says that with increasing the upstream distance, v tends to zero much faster than v_F. This is also well apparent in Figure 4.20a, where both velocities are plotted as functions of axial distance.

The question what happens if a portion of the wall is ventilated is more difficult to answer since, as we have pointed out before, the ventilated wall boundary conditions are generally unknown. It seems that the principle still holds, at least for "passive" wind tunnel walls where no

forced blowing or sucking is employed. In Figure 4.20b the same v_F as before is compared with v calculated using an assumption that $v=-u$ on the upper wall and $v=u$ on the lower wall. This relationship is a special case of the ideal porous-wall boundary condition $v \pm Pu = 0$ with porosity (permeability) parameter $P=1$. The formula which was used to generate the axial values of v was again obtained using the method of images (Ebihara [17]). We see that porosity $P>0$ makes convergence upstream of the vortex more rapid and downstream slow. If $P \to \infty$, corresponding to approaching the open jet condition $u=0$, the convergence of v upstream of the vortex improves further, but downstream of the vortex the flow becomes permanently deflected, see Figure 4.20c. Based on these and similar observations, the upstream conditions described by Eqs.(4.3.11) appear to be quite acceptable. It is of course realised that these conditions may lead to serious errors if imposed too close to the model (Akai and Piomelli, 1984). A more rigorous approach (at least on paper) is to actually measure the flow angles at some point, preferably non-intrusively.

As a point of interest, we may also mention that the complex-variable treatment of the 2D problem leads to the Schwarz problem (Smith [69]), consisting of determining an analytic function inside a domain from its defined real part on the boundary. Theory (e.g. Gakhov [24]) shows that the integration of the Cauchy-Riemann equations introduces an unknown imaginary constant that needs to be specified in order to make the solution unique. Translated into the language of aerodynamics: the flow angle constant is again unknown.

Last but not least in order of importance are the methods of measuring the perturbation u-velocity along the test section boundary. Since the wall correction method is based on potential-flow theory, the measurement should not be made on the wall itself, but at a distance where the effect of the wall boundary layer on static pressure is negligible. The simplest way to obtain u is by measuring static pressure on a plate (rail) instrumented with pressure orifices, as illustrated in Figure 4.21a. The plate is mounted on the wall in the direction parallel to mainstream. For isentropic flow in the x,z-plane it follows

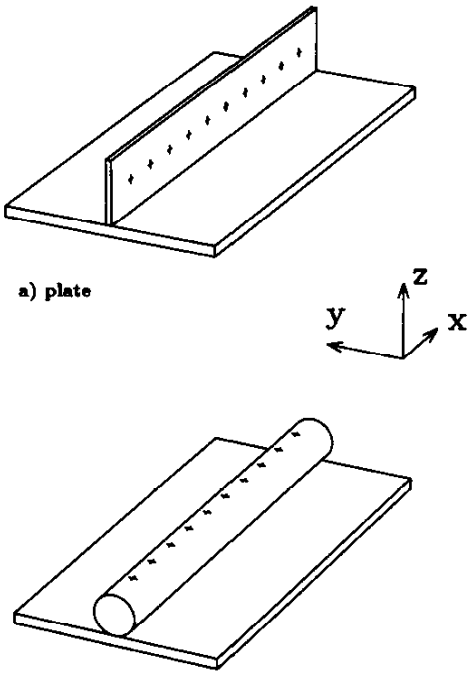

Figure 4.21 Schematic of devices with a single row of pressure orifices

$$C_P = \frac{2}{\gamma M_\infty^2}\left\{\left[1-\frac{\gamma-1}{2}M_\infty^2\left(\frac{U^2+W^2}{U_\infty^2}\right)\right]^{\frac{\gamma}{\gamma-1}}-1\right\} = -2u-u^2-w^2+\ldots$$

where C_P is the measured pressure coefficient and $u=\left(U-U_\infty\right)/U_\infty$ and $w=W/U_\infty$ are the components of the disturbance velocity in the x and z directions. the first-order approximation, valid throughout the whole subsonic-supersonic regime, is :

$$u=-\frac{1}{2}C_P \qquad (4.3.12)$$

If there is a lateral component of velocity (in the y-direction), the plate interacts with the flow and the measured pressure may no longer represent the local stream static pressure. For three-dimensional flows, a more suitable device is a pipe with a row of pressure orifices facing the test section interior, Figure 4.21b. The pipe also interacts with the ambient flow, but in a more predictable manner. Using slender body theory, Nenni et al. (1982) derived for a pressure coefficient on a circular cross-section pipe

$$C_p = -2u - \beta^2 u^2 + 2d\left(\frac{\partial v}{\partial x}\cos\omega + \frac{\partial w}{\partial x}\sin\omega\right) - 4\left(v\sin\omega - w\cos\omega\right)^2 \qquad (4.3.13)$$

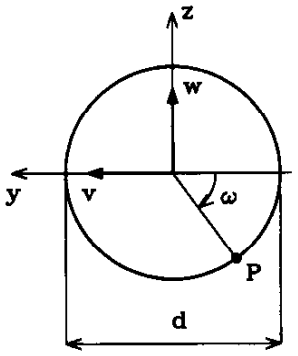

Figure 4.22 : Cross-flow plane of a circular pipe

where u, v, w are the components of disturbance velocity, d is the pipe diameter, and ω is the azimuthal angle of the pressure orifice P, as defined in Figure 4.22. For the orifices shown in Figure 4.21b the corresponding azimuthal angle is $\omega = 3\pi/2$. However, regardless of the azimuthal location of the pressure orifices, the transverse components of velocity v and w need to be known, in order to retrieve u from Eq.(4.3.13). This may be possible if the wall interference evaluation is arranged in an iterative fashion. The contributions of v and w and their derivatives can of course be eliminated by using several rows of pressure orifices (Nenni et al. [53]). A more serious objection to using Eq.(4.3.13) is that it has been derived for inviscid flow and would not apply should the pipe be immersed, partly or totally, in the wall boundary layer. In contrast, the linear approximation, as described by Eq.(4.3.12), may hold even then. Assuming that C_p is constant across the boundary layer in the direction normal to the wall, then the evaluated u represents the perturbation velocity on the outer edge of the boundary layer. Provided that the boundary displacement is small compared to the dimensions of the test section, the displacement may be neglected in routine wall interference computations.

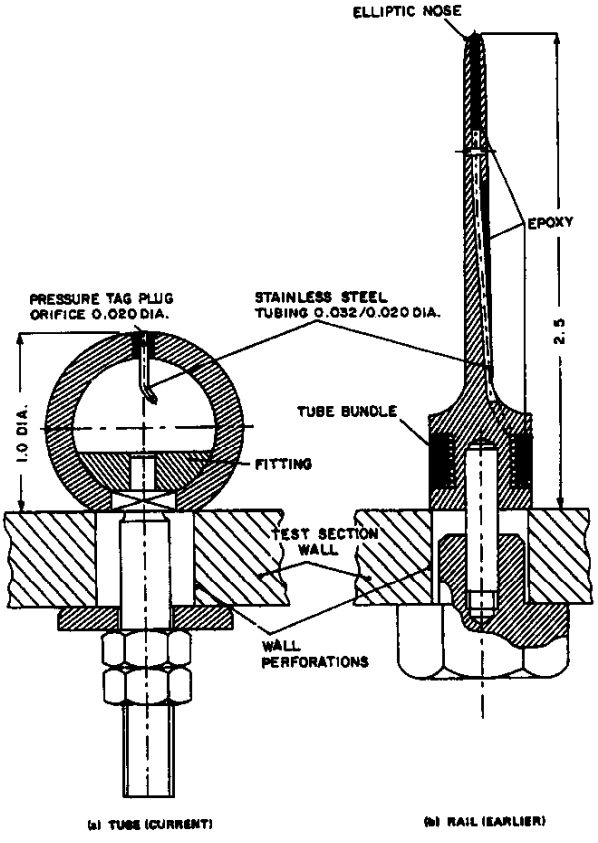

Figure 4.23 IAR Static pressure devices

A practical implementation of these static pressure devices is illustrated in Figure 4.23. The "rail" was the initial design used in early two-dimensional measurements in the High Speed Wind Tunnel in Ottawa (Peake et al. [57]). The impetus for its development came from an idea to supply the CFD method by Magnus and Yoshihara [44] by a pressure boundary condition, in an attempt to simulate computationally flow past an airfoil under the constraint of wind tunnel walls. Similar rails were subsequently built in a number of other facilities (Blackwell [9], Sawada [63], and Smith [68]) and used even for half-model (Pounds and Walker [59] and Hinson and Burdges [31], Goldhammer and Steinle [28]) and

full-model testing (Mokry and Galway [48]). Later, the rails were superseded by pipes (tubes), as they were easier to manufacture and also more suitable for three-dimensional testing. As discussed by Galway [25], the number and location of these pressure pipes depend upon the test section and model configuration, so that adequate definition of the pressure at the boundary surface through interpolation and extrapolation is possible. In the examples shown in Figure 4.24, a slightly irregular placement of the pipes was enforced by wall structural supports on the plenum side of the test section.

For slotted walls, where the mean-flow boundary conditions are established at greater distances from the walls, installation of pressure tubes or rails becomes less practical, although still feasible (Smith [69]). The inviscid slot flow analyses suggest that the pressure orifices need to located at least one slot spacing distance from the wall, in order not to be adversely affected by the rapidly varying flow in the slot (Smith [69], Kemp [36] and Steinle [73]). This hypothesis was verified experimentally by Everhart and Bobbitt [18]. For longitudinally slotted walls it is often more convenient to measure the boundary pressures using orifices installed directly in the slats, usually along or close to their centrelines (Sewall [64]). In determining the

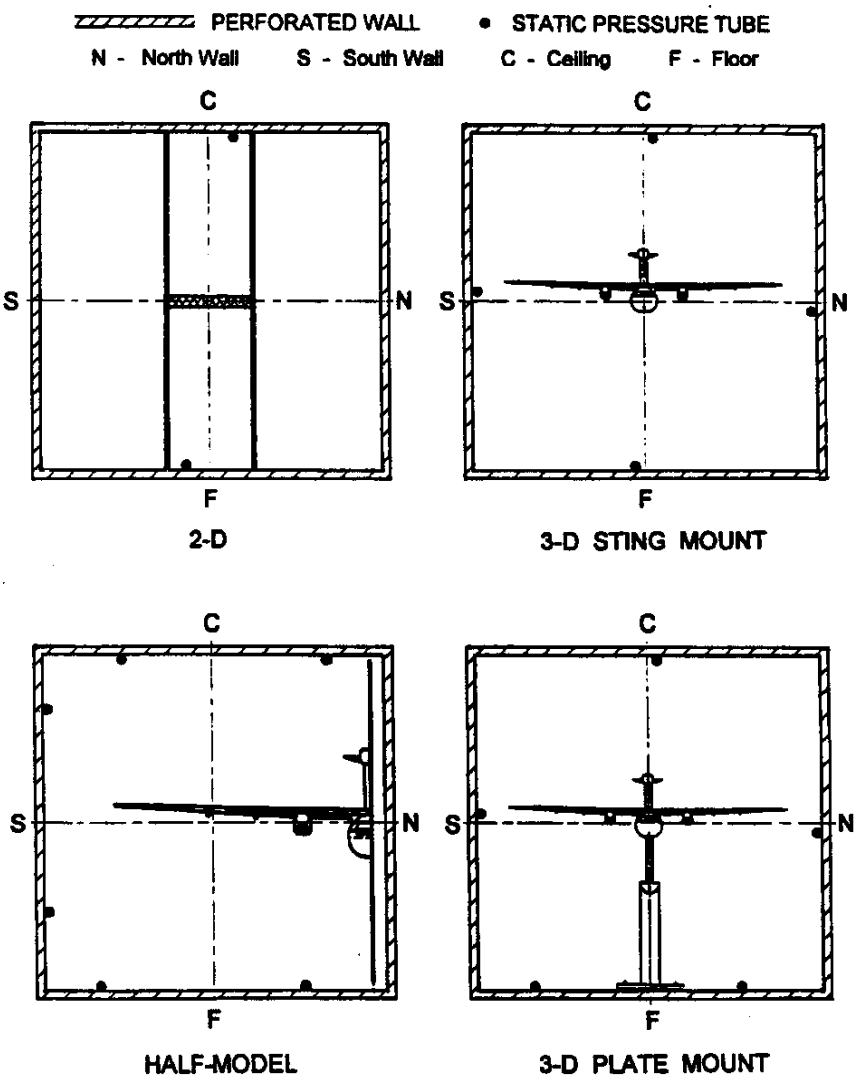

Figure 4.24 Location of static pressure tubes (pipes) for different modes of testing

streamwise component of perturbation velocity, u, it is necessary, in principle, to apply a correction to the value obtained from Eq.(4.3.12) when slat pressure coefficient is used as input. Based on the inviscid slot flow analysis by Berndt [7], Freestone et al. [22] deduced that for typical slotted wall geometry's the error of the mean value of u would not exceed 0.004 (0.4% of freestream velocity). This error estimate is consistent with earlier findings of Smith [69] and Firmin and Cook [20], implying that the pressure measurement made over the centre of the slat may be used as a reasonable approximate to the local mean static pressure at subsonic speeds. Unfortunately, there is also contradicting experimental evidence (GARTEur [26], and Everhart and Bobbitt [18]) that, depending on slot geometry and orifice locations, the differences between the slat pressures and mean static pressures can be more substantial. The conclusion to be drawn from this discussion is that, unless supported by supplementary flow measurements, pressure measured on the slats should not be presumed equal to the mean static pressure at the wall. A positive aspect of slat pressure measurement is that it is non-intrusive, in contrast to that provided by a static pressure pipe. Unfortunately, the effects of viscosity and vorticity in the immediate vicinity of the slotted wall generate very complex cross-flow patterns (Wu et al. [79]) that make a rigorous interpretation of the measured pressure data difficult.

Concerning the perforated walls, the measurement of pressure by orifices installed directly in the walls is even more problematic. For closely-spaced perforation holes the measured pressure suffers from a great deal of scatter even when the pressure orifices are positioned exactly at the same locations with respect to the surrounding perforation holes (Ohman and Brown [54]). This poses a problem especially for three-dimensional testing, where the pressure disturbances generated by the model are generally weak and hidden in the scatter generated by the holes. Since the scatter is spatially fixed, a partial remedy is in calculating the wall interference correction as an incremental one, using the differences of boundary pressures measured with model in and model out. Another possibility is to plug the perforation holes surrounding the pressure orifice, but this of course changes the local permeability of the wall. A variant of the perforated wall which avoids this problem is a porous-slotted wall comprised of a sufficient number of lines of porosity as to behave closely as a uniform porous wall such as the NASA Ames 11-by 11-Foot Transonic Tunnel. In this case, static pressure measurements can be made without affecting local porosity.

4.3.2 Two-Variable Method

The first successful evaluation of the 2-D interference flow field from two flow variables measured at the control surface was reported by Lo [42]. Both numerical demonstration and experimental verification are given in the same paper. The method uses the Fourier transform solution (Lo and Kraft [43]) for linearised subsonic flow past a nonlifting airfoil. A more straightforward Cauchy's integral approach to the two-variable method was subsequently described by Kraft and Dahm [38], Smith [69], and Amecke [3]. The general formulation of the method for 3-D flows, based on Green's identity, is due to Ashill and Weeks [4]; for more discussion see also Ashill and Keating [5]. A Fourier transform solution for the blockage interference, obtained as a function of two velocity components measured at a circular-cylinder surface, has recently been given by Qian and Lo [60].

The two-variable method for the ventilated-wall test sections is essentially the same as for the closed-wall test section described in Chapter 4.1.4 and 4.2.5.2. The only difference lies in the fact that the normal velocity at the solid wall is known, whereas for the ventilated walls it needs to be measured.

The wall interference potential obtained from Eq.(4.14) is

$$\phi_I = -\frac{1}{4\pi}\int_S \left[\frac{\partial\phi}{\partial n}\frac{1}{r} - \phi\frac{\partial}{\partial n}\left(\frac{1}{r}\right)\right] dS \qquad (4.3.14)$$

where ϕ_I is to be evaluated at an interior point $P(x_0, y_0, z_0)$ and r is a distance between this point and point $Q(x, y, z)$ that identifies the location of the surface element dS. The "observation" point P is held fixed, whereas Q is a "running" or "dummy" point in the integration's on the right-hand side of Eq.(4.3.14). As in Chapter 4.1, the normal derivatives are taken inward towards the working section. Physically, Eq.(4.3.14) can be interpreted as a surface distribution of sources of density $\partial\phi/\partial n$ and a surface distribution of doublets of density $(-\phi)$.

The two-dimensional analogue of Eq.(4.3.14) is (Labrujère et al., 1986)

$$\phi_I = -\frac{1}{2\pi}\int_C \left[\frac{\partial\phi}{\partial n}\ln\left(\frac{1}{r}\right) - \phi\frac{\partial}{\partial n}\ln\left(\frac{1}{r}\right)\right] ds \qquad (4.3.15)$$

where ds is the element of arc length of the boundary contour C. In two dimensions, ϕ can be differentiated in the direction tangent to the contour, so that the specification of ϕ is equivalent to specifying the tangential component of disturbance velocity, $\partial\phi/\partial s$. An alternative Cauchy-integral formulation of the two-variable method (Smith [69]) uses the complex disturbance velocity $u - iv$.

The number of velocity components needed to be measured in order to implement the two-variable method in three dimensions is again as the name of the method suggests: two. From ϕ defined on the bounding surface two components of tangential velocity can be derived; yet, if one of them is measured, the other is determined by integrating the irrotational-flow conditions. The second velocity component that needs to be measured is the normal one, $\partial\phi/\partial n$.

As discussed in Chapter 4.2, the two-variable method is most easily applied to solid wall test sections, where the normal velocity component, $\partial\phi/\partial n$, can be determined from the local slope of the boundary-layer displaced wall surface. If the test section walls are straight and the boundary layer growth is neglected, $\partial\phi/\partial n = 0$. In that case the source distribution drops out of Eq.(4.3.14) and the implementation of the method is particularly simple.

Before discussing the techniques for measuring $\partial\phi/\partial n$ in ventilated-wall wind tunnels, we shall set up a simple numerical model to illustrate how the method is supposed to work when both ϕ and $\partial\phi/\partial n$ participate. Integral (4.3.14) and its derivatives will be approximated as sums of contributions of constant-density panels, into which the boundary surface S is divided. The closed-form solutions for the contributions of a rectangular, unit-density source or doublet panel are given in the Appendix. What remains to be done is to change the co-ordinates from the local (panel) co-ordinate system to the global (test section) co-ordinate system, multiply the contributions by the local source and doublet densities, and then sum up all panel contributions. There is no system of equations as such to be solved in the two-variable method.

In the example shown in Figure 4.25a the test section is a simple right-angled box. The panels cover the top, bottom and side walls, and also the upstream and downstream faces. The plane $y = 0$ is assumed to be a plane of symmetry (a solid reflection plate in the half-model test arrangement). The division of

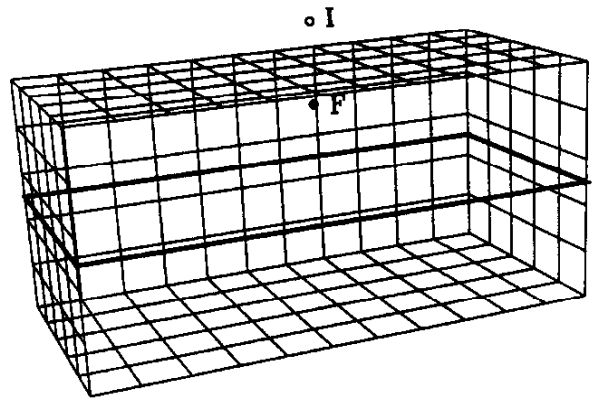

a) Paneling of the test section; singular points and observation plane

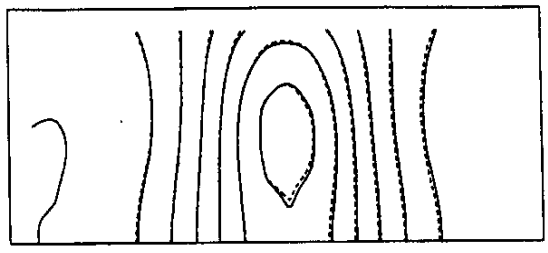

b) u-velocities induced by a doublet at point I

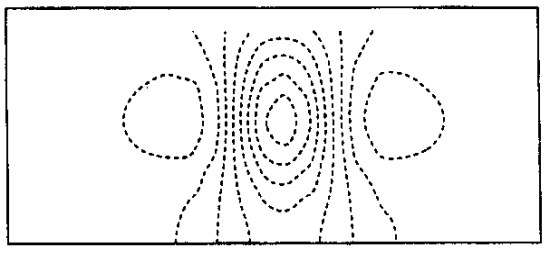

c) u-velocities induced by a doublet at point F

Figure 4.25 Processing of external and internal singularities by the two-variable method

the box in the x,y,z directions is $11\times5\times5$, making a total of 215 panels. Symmetry is built into the scheme by supplementing the contribution of each panel by its reflected counterpart.

Figure 4.25b shows the effect of a point doublet in the x-direction, located at point I outside the box. Superimposed with the uniform stream, the singularity is known to model incompressible flow past a sphere. The broken lines are the u-velocity contours induced by the doublet at the interior plane $z=0$. The solid lines are the contours produced by the two-variable method from the values of ϕ and $\partial\phi/\partial n$ generated by the doublet at the panel centroids. Apart from small numerical inaccuracies, the method is seen to have produced the effect of an external singularity $\phi=\phi_I$.

Figure 4.25c shows the effect of the same doublet placed the same distance from the wall at point F inside the box. The broken lines are still present, except that they are more dense because the doublet is now much closer to the observation plane than before. However, the solid lines have all disappeared. (Actually, there would still be numerical error contours; but the selected contour step was too large to capture them.) The two-variable method has thus eliminated the effect of an internal singularity, $\phi=\phi_F$.

A question arises whether the same also applies to potential-flow singularities other than doublets. The answer, which follows from Green's (third) identity, is affirmative. If we substitute in the integrand of Eq.(4.3.14) $\phi=\phi_I$, then the value of the integral will again be ϕ_I because ϕ_I is non-singular in the test section interior. However, if we set $\phi=\phi_F$, then the integral vanishes since ϕ_F is non-singular in the test section exterior. Accordingly, if the model is represented by internal singularities and the wind tunnel walls by the external singularities, the method will automatically account only for the external ones. This is exactly what is done when evaluating wall interference using the method of images: the summation is carried out over the whole infinite array of singularities and then the internal ones are subtracted. An interesting point is that the two-variable method does it by processing the measured boundary values of ϕ and $\partial\phi/\partial n$, regardless of whether or not the internal and external singularities can be reconstructed from them.

It is now also apparent that the above conclusions could have been obtained by examining Eq.(4.3.14) in the first place without resorting to any kind of numerical experimentation. However, the simple numerical box just described is in fact a prototype of a wall interference code that would, apart from minor geometrical modification, be used to correct measurements in an actual test section of a wind tunnel. The easiest way to check the code for errors and inaccuracies is by processing some well-defined singularities, exactly the same way as has been demonstrated. By further modifying this numerical experiment one can also determine how many panels are needed to represent the walls adequately, how many measurement points are required and where they should preferably be located, how the interpolations should be set up, whether the integrals over the upstream and downstream ends could possibly be dropped (Labrujère et al. [41]), and so on. As we have already mentioned, the method is simple in principle, but there are many possibilities of how it could be implemented, each of them giving somewhat different answers.

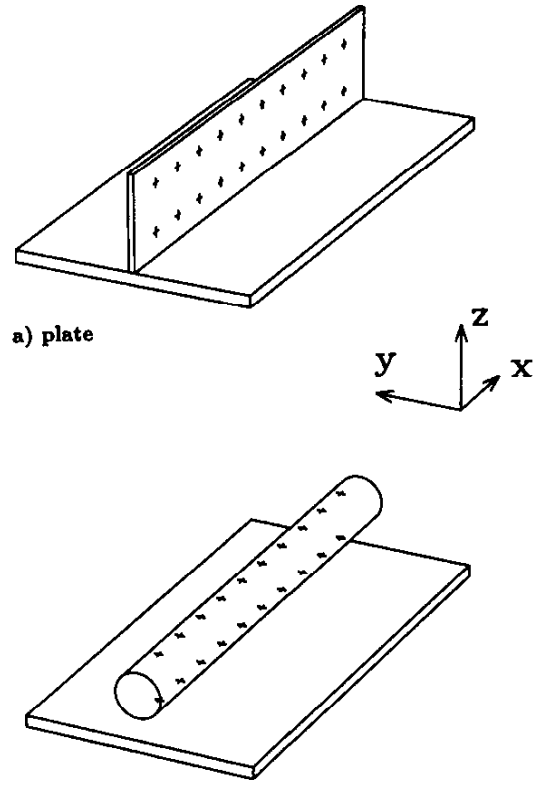

a) plate

b) pipe

Figure 4.26 Schematic of devices with two rows of pressure orifices

The simplest device for measuring two components of velocity is a plate with two rows of pressure orifices, aligned with the direction of mainstream, as shown schematically in Figure 4.26a. Assuming that the plate is in the x,y-plane where the x-axis is parallel with the orifice rows, we obtain (for small pressure perturbations) midway between the orifices

$$u = \frac{1}{2}(u_1 + u_2) = -\frac{1}{4}(C_{P1} + C_{P2}) \tag{4.3.16}$$

and, from the irrotational-flow condition,

$$\frac{\partial w}{\partial x} = \frac{\partial u}{\partial z} = \frac{u_2 - u_1}{d} = \frac{C_{P1} - C_{P2}}{2d}, \tag{4.3.17}$$

where d is the distance of the orifice rows.

A better device, especially for three-dimensional testing, is the double-orifice tube, also known as the Calspan pipe (Nenni et al. [53], Smith [70]), see Figure 4.26b. The pipe is equipped with two diametrically opposing rows of orifices, one facing the test section interior and the other one the wall. Substituting $\omega = \pi/2$ and $\omega = 3\pi/2$ in Eq.(4.3.13), we obtain respectively

$$C_{P1} = -2u - \beta^2 u^2 + 2d\frac{\partial w}{\partial x} - 4v^2$$

$$C_{P2} = -2u - \beta^2 u^2 - 2d\frac{\partial w}{\partial x} - 4v^2 \ .$$

Adding and subtracting these expressions and retaining only the highest-order terms, we find that u is again approximated by Eq.(4.3.16); but, for the streamwise derivative of the normal velocity it follows:

$$\frac{\partial w}{\partial x} = \frac{C_{P1} - C_{P2}}{4d} \qquad (4.3.18)$$

where d is the tube diameter. Comparing Eqs.(4.3.17) and (4.3.18) we see that for the same $\partial w/\partial x$ and distances, d, of the orifices, the Calspan pipe doubles the pressure difference which otherwise would be measured by the dual-orifice plate. This amplification is especially welcome when the measured pressure differences are of the same magnitude as the discrete perturbations emanating at the ventilated walls (Smith [70]), or in low speed wind tunnels, where the pressure differences are weak in general (Fernkrans [19]).

In either case, the w-velocity has to be obtained from its derivative by integration, and there re-appears again the familiar problem of determination of an unknown integration constant. Nenni et al. (1982) describe the steps to be taken as follows: assuming that w is known at a reference station x_R, then $\partial w/\partial x$ can be integrated to give

$$w(x) = w(x_R) + \int_{x_R}^{x} \frac{\partial w}{\partial x} dx \qquad (4.3.19)$$

If w can be measured at a suitable reference point, the pressure distributions along the top and bottom of the pipe can also be used to determine w, in addition to u. This supplementary measurement of $w(x_R)$ has to be made by an alternative measuring technique, or else x_R has to be chosen where $w(x_R)$ is expected to be zero. As the major shortcomings of measuring flow direction by the Calspan pipe identified were: weak pressure differences and reliance on slender-body theory, which ignores the possible effects of viscosity and flow non-uniformity in the vicinity of the walls (Smith [70]).

Because half the (diametrically opposing) orifices face the wall, the pipe has to be positioned some distance from the wall. A typical example is in Figure 4.27, showing an installation of a Calspan pipe in the NLR Pilot Tunnel (GARTEur [26]). An interesting concept for three-dimensional testing is the AEDC rotating pipe system (Parker and Erickson [55] and Sickles [65]), shown in Figure 4.28. The system consists of two pipes and a mechanism that can rotate them about the centreline of the perforated-wall test section (AEDC Tunnel 4T). The pipes sweep out a cylindrical measurement surface, approximately one inch from the wall at the closest point. Each 5/8-inch diameter pipe is equipped with 40 pairs of diametrically opposing orifices, distributed more densely where large pressure gradients are expected. The pressure and the difference in the pressures for each pair are used to determine the components of velocity in the streamwise and radial directions. The integration to determine the longitudinal distribution of the radial component of velocity is performed over two intervals: from upstream to peak suction pressure, and (backward) from downstream to peak suction pressure. The integration constants for the two regions are measured by upstream and downstream flow angle probes, also visible in Figure 4.28. A more detailed discussion of the apparatus and sample measurements can be found in Kraft et al. [39].

For slotted walls, it has also been suggested to measure or establish the mean flow boundary conditions from velocities measured by probes traversed inside the slots (Freestone and Mohan [23]). Provided that the streamwise variations of the mean normal velocity are relatively slow, as most experiments confirm, a

probe traverse could be substituted by a number of fixed flow angle probes (Mohan and Freestone, [46]), making the technique suitable even for production wind-tunnel testing.

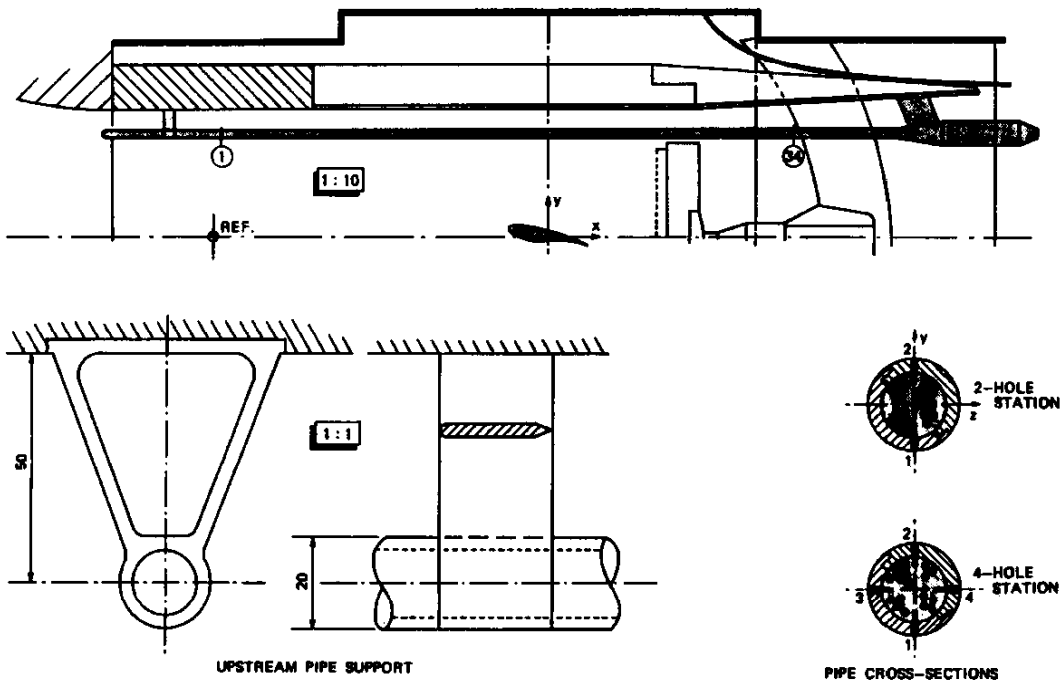

Figure 4.27 Calspan pipe and its mounting in the NLR Pilot Tunnel

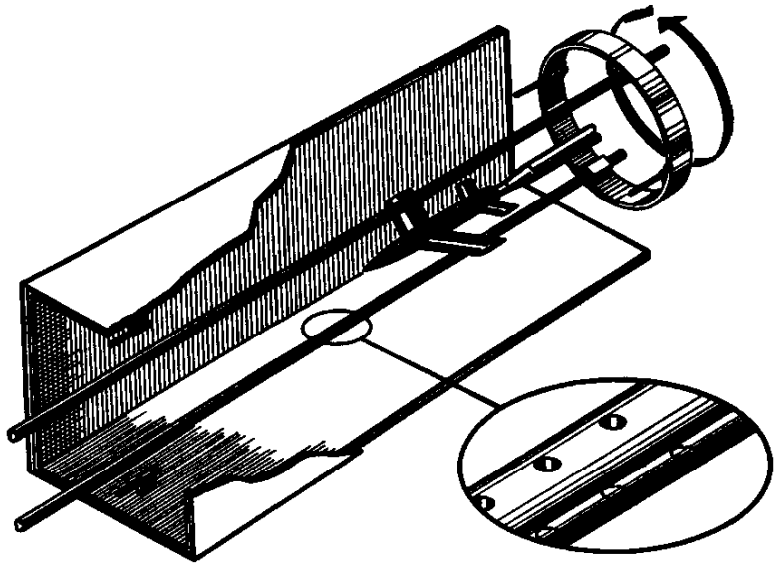

Figure 4.28 AEDC Two-Variable Measuring System

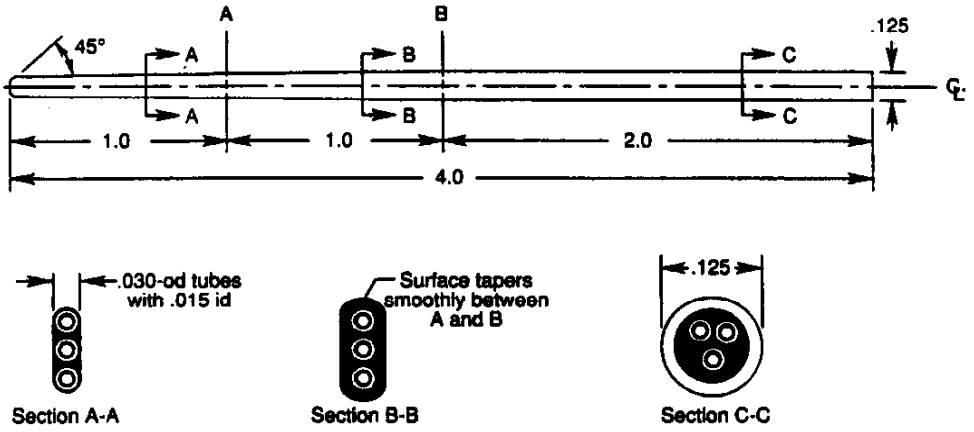

Figure 4.29 NASA/United Sensor flow angle probe

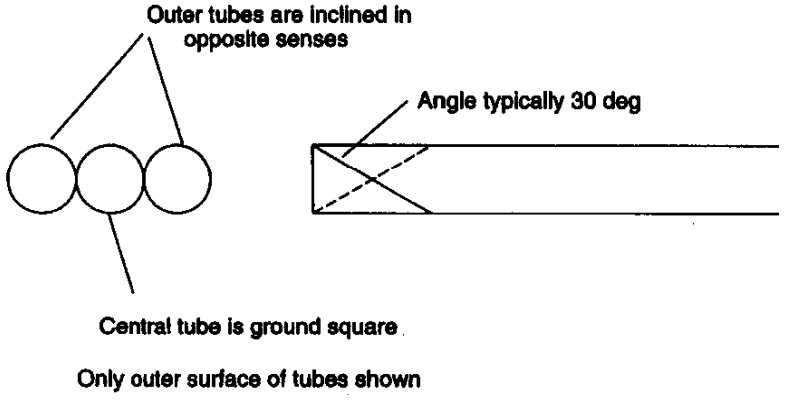

Figure 4.30 Sketch of in-line probe to measure flow angle in presence of shear (Courtesy of M.M. Freestone)

A typical three-tube flow angle probe, used by Everhart and Bobbitt [18] for slot flow measurements in the NASA Langley 6 × 19 Inch Transonic Tunnel, is shown schematically in Figure 4.29. In an effort to eliminate the error when crossing the shear layer, Freestone has recently developed a flow angle probe, whose pressure-measuring tubes are positioned parallel to the wall, see Figure 4.30.

The velocity component normal to the wall normal is quite substantial inside the slot and all indications are that it can be measured very accurately. A difficulty arises when one wishes to establish correspondence between the velocity inside the slot and the mean or "homogeneous" normal velocity at the wall that enters Eq.(4.3.14) or (4.3.15). In theory, the latter can be evaluated by laterally averaging the mass flux using the slender-body theory (Everhart and Bobbitt [18]). Unfortunately, viscous effects in the slots do not just manifest themselves by narrowing the effective slot width (vena contracta). Experimental data show that along the slot segments where air is flowing into the test section, rather than out of it, the crossflow is causing a rapid thickening of the wall boundary layer. This effective amplification of the mean normal velocity over the inflow regions of the walls was found to be of up to about 4.0 (Freestone and Mohan [23]). Quantitative observations of similar kind, both in slotted and perforated walls, have also been made by Vidal et al. [78], Chan [11], Firmin and Cook [20], and Crites and Rueger [15]. Freestone (private communication, 1995) suggests: "It is possible in principle to make a series of measurements in the test section of interest, specially designed to provide the amplification factor in sufficient detail for subsequent application. Whether or not it would be feasible or practical undertaking is not so clear. Much may depend on first demonstrating that it is not necessary to know the streamwise variations in boundary layer thickness very precisely in order to achieve the desired accuracy of wall interference. Perhaps it would be adequate to know the overall increase in thickness over the length of the inflow region, but even this, in a three-dimensional test, is no small task." Another possibility

is keeping the amplification factor close to unity by enforcing outflow above and below the model and returning the drawn air to the wind-tunnel circuit some distance downstream (Mohan and Freestone [46]). Of course, the corresponding pressure gradient can make the measured model data difficult to correct to free stream conditions.

In spite of the current difficulties in measuring the normal component of velocity at the wind tunnel boundary, the uncertainty of the model representation inherent in the one-variable method is a far more serious problem, especially in transonic or separated flow regimes. As spelled out by Rubbert [62] and the GARTEur Report [26], attention will undoubtedly turn more and more to the two-variable method, which is capable of producing corrections from two components of boundary velocity, without knowing anything about the flow in the neighbourhood of the model. Since the relative accuracy or dependability of the two-variable method is a function of measurement accuracy's inherent in producing the two components of velocity near the walls, it is predominantly in improving the measurement techniques where progress can be made.

4.3.3 Alternative Methods

There are other methods of utilising boundary measurements in the evaluation of subsonic wall interference besides those discussed in this Chapter, but most of them are not as direct as those described above. An attractive approach, at least from the production-testing viewpoint, is to use the two-variable method with the measurement of one variable. This is of course possible only if the wall boundary condition is known, so that the unknown variable (normal velocity) can be derived from the measured one (pressure). An example of this approach is discussed by Rueger and Crites, et. al. (1994.) In this approach the uncertainty of model representation, inherent in the one-variable method, is traded for the uncertainty in the wall boundary condition. The boundary condition at a given wall location can be established, for example, by applying the one-variable method in instances when the model far field can be well predicted (subcritical, low incidence flow). In essence, the evaluation of the transverse velocity components v_I and w_I consists of streamwise integrating Eqs.(4.3.10), where the derivatives of u_I have been obtained by the one-variable method. The subsequent two-variable evaluation is used in flow situations where the far-field of the model cannot be predicted as reliably (high incidence or supercritical flow).

Appendix: Rectangular Wall Panel

Considered is a rectangular panel

$$R = \left\{(x, y, z): x_1 \le x \le x_2,\ y_1 \le y \le y_2,\ z = 0\right\},$$

whose normal is oriented along the positive z-axis and whose source or doublet density is unity. The distance of the observation point x_0, y_0, z_0 from the panel point x, y, z is

$$r = \sqrt{(x_0 - x)^2 + (y_0 - y)^2 + (z_0 - z)^2}\ .$$

Evaluation of the potential and its derivatives induced by the panel at the observation point can be quite tedious (Hess and Smith [30], Holst [32], Katz and Plotkin [35]) but the results can be manipulated into neat, Biot-Savart-type formulae.

For the source panel, we obtain

$$-\int_R \frac{1}{r}\,dS = (x_0 - x_2)(u^s_{22} - u^s_{21}) + (x_0 - x_1)(u^s_{11} - u^s_{12}) + (y_0 - y_2)(v^s_{22} - v^s_{12}) +$$

$$+ (y_0 - y_1)(v^s_{11} - v^s_{21}) + z_0(w^s_{11} - w^s_{21} + w^s_{22} - w^s_{12})$$

$$-\frac{\partial}{\partial x_0}\int_R \frac{1}{r}\,dS = u^s_{11} - u^s_{21} + u^s_{22} - u^s_{12}$$

$$-\frac{\partial}{\partial y_0}\int_R \frac{1}{r}\,dS = v^s_{11} - v^s_{21} + v^s_{22} - v^s_{12}$$

$$-\frac{\partial}{\partial z_0}\int_R \frac{1}{r}\,dS = w^s_{11} - w^s_{21} + w^s_{22} - w^s_{12}$$

where

$$u^s_{ij} = \ln\left[r_{ij} - (y_0 - y_j)\right]$$

$$v^s_{ij} = \ln\left[r_{ij} - (x_0 - x_i)\right]$$

$$w^s_{ij} = \arctan\frac{(x_0 - x_i)(y_0 - y_j)}{z_0\, r_{ij}}$$

and

$$r_{ij} = \sqrt{(x_0 - x_i)^2 + (y_0 - y_j)^2 + z_0^2}\ .$$

The normal velocity induced by a source panel has a jump discontinuity across the panel: if $x_1 < x_0 < x_2$, $y_1 < y_0 < y_2$ and $z_0 \to 0\pm$,

$$-\frac{\partial}{\partial z_0}\int_R \frac{1}{r}\,dS \to \pm 2\pi\ .$$

The tangential velocities and the potential itself are continuous across the panel.

For the doublet panel, similarly,

$$\int_R \frac{\partial}{\partial z}\left(\frac{1}{r}\right)dS = -\frac{\partial}{\partial z_0}\int_R \frac{1}{r}\,dS = w^s_{11} - w^s_{21} + w^s_{22} - w^s_{12}$$

$$\frac{\partial}{\partial x_0}\int_R \frac{\partial}{\partial z}\left(\frac{1}{r}\right)dS = u^d_{11} - u^d_{21} + u^d_{22} - u^d_{12}$$

$$\frac{\partial}{\partial y_0}\int_R \frac{\partial}{\partial z}\left(\frac{1}{r}\right)dS = v_{11}^d - v_{21}^d + v_{22}^d - v_{12}^d$$

$$\frac{\partial}{\partial z_0}\int_R \frac{\partial}{\partial z}\left(\frac{1}{r}\right)dS = w_{11}^d - w_{21}^d + w_{22}^d - w_{12}^d$$

where

$$u_{ij}^d = \frac{z_0(y_0 - y_j)}{[(x_0 - x_i)^2 + z_0^2]\, r_{ij}}$$

$$v_{ij}^d = \frac{z_0(x_0 - x_i)}{[(y_0 - y_j)^2 + z_0^2]\, r_{ij}}$$

$$w_{ij}^d = -\frac{(x_0 - x_i)(y_0 - y_j)}{(x_0 - x_i)^2(y_0 - y_j)^2 + z_0^2\, r_{ij}^2}\left(r_{ij} + \frac{z_0^2}{r_{ij}}\right).$$

The potential of the doublet panel has a jump discontinuity across the panel: if $x_1 < x_0 < x_2$, $y_1 < y_0 < y_2$ and $z_0 \to 0\pm$,

$$\int_R \frac{\partial}{\partial z}\left(\frac{1}{r}\right)dS \to \pm 2\pi .$$

The velocity components are continuous.

REFERENCES TO CHAPTER 4.3

[1] Akai, T.J and Piomelli, U., 1984, "Effect of Upstream Parallel Flow on Two-Dimensional Wind-Tunnel Tests," AIAA-84-2153.

[2] Al-Saadi, J.A., 1991, "Model Representation in the PANCOR Wall Interference Assessment Code," NASA TM-104152.

[3] Amecke, J., 1985, " Direkte Berechnung von Wandinterferenzen und Wandadaptation bei zweidimensionaler Strömung in Windkanälen mit geschlossenen Wänden," DFVLR-FB 85-62; also translated as NASA TM-88523, 1986.

[4] Ashill, P.R. and Weeks, D.J., 1982, "A Method for Determining Wall-Interference Corrections in Solid-Wall Tunnels from Measurements of Static Pressure at the Walls," AGARD-CP-335, pp.1.1 - 1.12.

[5] Ashill, P.R. and Keating, R.F.A., 1988, "Calculation of Tunnel Wall Interference from Wall-Pressure Measurements," The Aeronautical Journal of the Royal Aeronautical Society, pp.36-53.

[6] Aulehla, F., 1977, "Drag Measurement in Transonic Wind Tunnels," AGARD-CP-242, pp.7.1-7.18

[7] Berndt, S.B., 1982, "Measuring the Flow Properties of Slotted Test-Section Walls," FFA 135, The Aeronautical Research Institute of Sweden.

[8] Binion, T.W. and Lo, C.F., 1972, "Application of Wall Corrections to Transonic Wind Tunnel Data," AIAA-72-1009.

[9] Blackwell, J.A., 1979, "Wind-Tunnel Blockage Correction for Two-Dimensional Transonic Flow," Journal of Aircraft, Vol.16, No.4, pp.256-263.

[10] Capelier, C., Chevallier, J.P., and Bouniol, F., 1978, "Nouvelle méthode de correction des effets de parois en courant plan," La recherche aérospatiale, Jan.-Feb. 1978, pp.1-11; also translated as ESA-TT-491, 1978.

[11] Chan, Y.Y., 1981, "Analysis of Boundary Layers on Perforated Walls of Transonic Wind Tunnels," Journal of Aircraft, Vol.18, pp.469-473.

[12] Chen, C.F. and Mears, J.W., 1957, " Experimental and Theoretical Study of Mean Boundary Conditions at Perforated and Longitudinally Slotted Walls," Tech. Rep. WT-23, Brown University.

[13] Chevallier, J.P., 1984, "Survey of ONERA Activities on Adaptive-Wall Applications and Computation of Residual Corrections," Wind Tunnel Wall Interference Assessment/Correction 1983, NASA CP 2319, pp.43-58.

[14] Cole, J.D. and Cook, L.P., 1986, "Transonic Aerodynamics," North-Holland, pp.259-272.

[15] Crites, R. and Rueger, M., 1992, "Modeling the Ventilated Wind Tunnel Wall, AIAA 92-0035.

[16] Crites, R. and Steinle, F.W., Jr., 1995, "Wall Interference Reduction Methods for Subsonic Wind Tunnels", AIAA 95-0107.

[17] Ebihara, M., 1972, "A Study of Subsonic Two-Dimensional Wall-Interference Effect in a Perforated Wind Tunnel with Particular Reference to the NAL 2m × 2m Transonic Wind Tunnel,"TR-252T, National Aerospace Laboratory, Tokyo.

[18] Everhart, J.L. and Bobbitt, P.J., 1994, "Experimental Studies of Transonic Flow Field Near a Longitudinally Slotted Wind Tunnel Wall," NASA Technical Paper 3392.

[19] Fernkrans, L., 1993, "Calculation of Low Speed Wind Tunnel Wall Interference from Static Pressure Pipe Measurements," AGARD-CP-535, pp.23.1-23.7.

[20] Firmin, M.C.P. and Cook, T.A., 1968, "Detailed Exploration of the Compressible Viscous Flow over Two-Dimensional Aerofoils at High Reynolds Numbers," ICAS Paper 68-09.

[21] Firmin, M.C.P. and Cook, P.H., 1983, "Disturbances from Ventilated Tunnel Walls in Aerofoil Testing," AGARD-CP-348, pp. 8.1-8.15.

[22] Freestone, M.M., Lock, R.C., and Mohan, S.R., 1991, "Determination of Wind Tunnel Interference Due to Slotted Wall Liners," MED/AERO Rept. No.179, City University, London.

[23] Freestone, M.M. and Mohan, S.R., 1993, "Interference Determination for Wind Tunnels With Slotted Walls," AGARD-CP-535, pp.19.1-19.12.

[24] Gakhov, F.D., 1966, "Boundary Value Problems," Pergamon Press.

[25] Galway, R.D., 1994, "Measurement of Low Level Pressure Disturbances in Proximity to a Perforated Wall in a Blowdown Wind Tunnel," presented at the 81st. Semi-annual Meeting of the Supersonic Tunnel Association, Buffalo, N.Y.

[26] GARTEur Action Group AD(AG-23), 1983,

[27] "Two-Dimensional Transonic Testing Methods," NLR TR 83086 U.

[28] Goldhammer, M.I. and Steinle, F.W., Jr., 1990, "Design and Validation of Advanced Transonic Wings Using CFD and Very High Reynolds Number Wind Tunnel Testing," ICAS 90-26.2.

[29] Gopinath, R., 1985, "Wall Interference Studies in 3-D Flows," TM-AE-8508, National Aeronautical Laboratory, India.

[30] Hess, J.L. and Smith, A.M.O., 1966, "Calculation of Potential Flow About Arbitrary Bodies," Progress in Aeronautical Sciences, Vol.8, pp.1-138.

[31] Hinson, B.L. and Burdges, K.P., 1981, "Evaluation of Three-Dimensional Transonic Codes Using New Correlation-Tailored Test Data," Journal of Aircraft, Vol.18, No.10, pp.855-861.

[32] Holst, H., 1990, "Verfahren zur Bestimmung von dreidimensionalen Windkanalwandinterferenzen und Wandadaptionen mit Hilfe gemessener Wanddrücke bei kompressibler Unterschallströmung," DLR-FB 0-46.

[33] Jacocks, J.L., 1976, "An Investigation of the Aerodynamic Characteristics of Ventilated Test Section Walls for Transonic Wind Tunnels," Doctoral Thesis, The University of Tennessee.

[34] Jones, D.J., 1979, "A Method for Computing 2-D Wind Tunnel Wall Interference Effects Allowing for Variable Porosity along Floor and Ceiling," LTR-HA-37, National Aeronautical Establishment, National Research Council Canada.

[35] Katz, J. and Plotkin, A., 1991, "Low-Speed Aerodynamics," McGraw-Hill, pp.282-288.

[36] Kemp, W.B., 1985, "A Slotted Test Section Numerical Model for Interference Assessment," Journal of Aircraft, Vol.22, No.3, pp.216-222.

[37] Kemp, W.B., 1990, "User's Guide to PANCOR: A Panel Method for Interference Assessment Method for a Slotted-Wall Wind Tunnel," NASA CR-4352.

[38] Kraft, E.M. and Dahm, W.J.A., 1982, "Direct Assessment of Wall Interference in a Two-Dimensional Subsonic Wind Tunnel," AIAA-82-0187.

[39] Kraft, E.M., Ritter, A., and Laster, M.L., 1986, "Advances at AEDC in Treating Transonic Wind Tunnel Wall Interference," ICAS-86-1.6.1.

[40] Labrujère, T.E., Maarsingh, R.A., and Smith, J., 1986, "Wind Tunnel Wall Influence Considering Two-Dimensional High-Lift Configurations," Journal of Aircraft, Vol.23, pp.118-125.

[41] Labrujère, T.E., Maarsingh, R.A., and Smith, J., 1988, "Evaluation of Measured-Boundary-Condition Methods for 3D Subsonic Wall Interference," NLR TR 88072 U.

[42] Lo, C.F., 1978, "Tunnel Interference Assessment by Boundary Measurements," AIAA Journal, Vol.16, No.4, pp.411-413.

[43] Lo, C.F. and Kraft, E.M., 1978, "Convergence of the Adaptive-Wall Wind Tunnel," AIAA Journal, Vol. 16, pp.67-72.

[44] Magnus, R. and Yoshihara, H., 1972, "Steady Inviscid Transonic Flows over Planar Airfoils - A Search for a Simplified Procedure," NASA CR-2186.

[45] Matyk, G.E. and Kobayashi, Y., 1977, "An experimental Investigation of Boundary Layer and Crossflow Characteristics of the Ames 2-by 2-Foot and 11- by 11-Foot Transonic Wind-Tunnel Walls," NASA T.M. 73257.

[46] Mohan, S.R. and Freestone, M.M., 1994, "Interference Determination for Three-Dimensional Flows in Slotted-Liner Wind Tunnels," ICAS-94-3.3.1.

[47] Mokry, M., Peake, D.J., and Bowker, A.J., 1974, "Wall Interference on Two-Dimensional Supercritical Airfoils, Using Wall Pressure Measurements to Determine the Porosity Factors for Tunnel Floor and Ceiling," LR-575, National Aeronautical Establishment, National Research Council Canada.

[48] Mokry, M. and Galway, R.D., 1977, "Analysis of Wall Interference Effects on ONERA Calibration Models in the NAE 5-ft. × 5-ft, Wind Tunnel," LR-594, National Aeronautical Establishment, National Research Council Canada.

[49] Mokry, M. and Ohman, L.H., 1980, "Application of the Fast Fourier Transform to Two-Dimensional Wind Tunnel Wall Interference," Journal of Aircraft, Vol.17, pp.402-408.

[50] Mokry, M., 1982, "Subsonic Wall Interference Corrections for Finite-Length Test Sections Using Boundary Pressure Measurements," AGARD-CP-335, pp.10.1 - 10.15.

[51] Mokry, M., 1985, "Subsonic Wall Interference Corrections for Half-Model Tests Using Sparse Wall Pressure Data," LR-616, National Aeronautical Establishment, National Research Council Canada.

[52] Mokry, M., Digney, J.R., and Poole, R.J.D., 1987, "Doublet-Panel Method for Half-Model Wind-Tunnel Corrections," Journal of Aircraft, Vol.24, pp.322-327.

[53] Nenni, J.P., Erickson, J.C., and Wittliff, C.E., 1982, "Measurement of Small Normal Velocity Components in Subsonic Flows by Use of Static Pipe," AIAA Journal, Vol.20, pp.1077-1083.

[54] Ohman, L.H. and Brown, D., 1990, "Performance of the New Roll-In Roll-Out Transonic Test Sections of the NAE 1.5m x 1.5m Blowdown Wind Tunnel," ICAS-90-6.2.2.

[55] Parker, R.L. and Erickson, J.C., 1982, "Development of a Three-Dimensional Adaptive Wall Test Section with Perforated Walls," AGARD-CP-335, pp.17.1-17.14.

[56] Paquet, J.B., 1979, "Perturbations induites par les parois d'une soufflerie - méthodes intégrales," Thèse Ing. Doc., Université de Lille, 1979.

[57] Peake, D.J., Bowker, A.J., Mokry, M., Yoshihara, H., and Magnus, R., 1974, "Transonic Lift Augmentation of Two-Dimensional Supercritical Aerofoils by Means of Aft Camber, Slot Blowing and Jet Flaps, in High Reynolds Number Flow, " ICAS Paper No.74-11.

[58] Piat, J.F., 1994, "Calculs des effets de parois dans des veines à parois perforées avec un code de singularités surfaciques," AGARD-CP-535, pp.27.1-27.12.

[59] Pounds, G.A. and Walker, J., 1980, "Semispan Model Testing in a Variable Porosity Transonic Wind Tunnel," AIAA-80-0461.

[60] Qian, X. and Lo, C.F., 1994, "Two-Variable Method for Blockage Wall Interference in a Circular Tunnel," Journal of Aircraft, Vol.31, No.5, pp.1130-1134.

[61] Rizk, M.H. and Smithmeyer, M.G., 1982, "Wind-Tunnel Interference Corrections for Three-Dimensional Flows," Journal of Aircraft, Vol.19, pp.465-472.

[62] Rubbert, P.E., 1981, "Some Ideas and Opportunities Concerning Three-Dimensional Wind-Tunnel Wall Corrections," Wind-Tunnel / Flight Correlation - 1981, NASA Conference Publication 2225, pp.217-229.

[63] Sawada, H., 1980, "A New Method of Calculating Corrections for Blockage Effects in Two-Dimensional Wind Tunnel with Ventilated Walls, Using Wall Pressure Measurements," Transactions of the Japan Society for Aeronautical And Space Sciences, Vol.22, No.61, pp.155-168.

[64] Sewall, W.G., 1984, ``Wall Pressure Measurements for Three-Dimensional Transonic Tests," AIAA-84-0599.

[65] Sickles, W.L., 1983, "A Data Base for Three-Dimensional Wall Interference Code Evaluation," NASA CP-2319, pp.101-115.

[66] Sickles, W.L. and Erickson, J.C., 1990, "Wall Interference Corrections for Three-Dimensional Transonic Flows," AIAA 90-1408.

[67] Smith, J., 1976, "Results of a Preliminary Investigation on 2-Dimensional Ventilated-Wall Interference, Based on an Analysis of Plenum Pressure Behaviour," Memorandum AC-76-012, National Aerospace Laboratory NLR.

[68] Smith, J., 1981, "A Method for Determining 2D Wall Interference on an Aerofoil from Measured Pressure Distributions near the Walls and on the Model," NLR TR 81016 U.

[69] Smith, J., 1982, "Measured Boundary Conditions Methods for 2D Flow," AGARD-CP-335, pp.9.1 - 9.15.

[70] Smith, J., 1985, "2D Wall Interference Assessment Using Calspan Pipes," NLR TR 85065 U.

[71] Stakgold, I., 1968, "Boundary Value Problems of Mathematical Physics," Vol.II, Macmillan.

[72] Starr, R.F., 1978, "Experimental Observations of Wall Interference at Transonic Speeds," AIAA 78-164.

[73] Steinle, F.W., Jr. and Stanewsky, E., 1982, "Wind Tunnel Flow Quality and Data Accuracy Requirements," AGARD-AR-184.

[74] Theodorsen, T., 1931, "The Theory of Wind-Tunnel Wall Interference," NACA Rept.410.

[75] Ulbrich, N. and Steinle, F.W., Jr., 1994, "Real-Time Wall Interference Calculations in three-dimensional Subsonic Wind Tunnel Testing," AIAA 94-0771.

[76] Ulbrich, N. and Steinle, F.W., Jr., 1995, "Semispan Model Wall Interference Prediction Based on the Wall Signature Method," AIAA 95-0793.

[77] Vaucheret, X., 1982, "Améliorations des calculs des effets de parois dans les souffleries industrielles de l'ONERA," AGARD-CP-335, pp.11.1-11.12.

[78] Vidal, R.J., Erickson, J.C., and Catlin, P.A., 1975, "Experiments with Self-Correcting Wind Tunnel," AGARD-CP-174, pp.11.1-11.13.

[79] Wu, J.M., Collins, F.G., and Bhat, M.K., 1983, "Three-Dimensional Flow Studies on a Slotted Transonic Wind Tunnel Wall," AIAA Journal, Vol.21, pp.999-1005.

[80] Steinle, F.W., Jr., „Development of the Porous-Slot Geometry of the NWTC Test Section", AIAA 07-0097